A pangenomics-enabled platform for the high-throughput discovery of antifungal resistance factors in crop pathogens

Guido Puccetti[1,2], Daniel Flückiger[2], Dominique Edel[2], Camille Delude[2], Sabina Moser Tralamazza[1], Thomas Badet[1], Gabriel Scalliet[2, §], Daniel Croll[1, §]

[1] Laboratory of Evolutionary Genetics, Institute of Biology, University of Neuchâtel, CH-2000, Neuchâtel, Switzerland

[2] Syngenta Crop Protection AG, Stein, Switzerland

[§] Jointly supervised the work

Correspondence: gabriel.scalliet@syngenta.com; daniel.croll@unine.ch

Author contributions: GP, GS and DC conceived the study, GP performed the research and analyzed the data. GP, DF, DE and CD performed analyses. SFFT provided materials. TB and SMT provided datasets. GS and DC supervised the work and acquired funding. GP, DC and GS wrote the manuscript.

Abstract

The rise of antifungal resistance is a global challenge for both human health and food security, because resistance emergence easily outpaces the antifungal development pipeline. Furthermore, resistance arises often in parallel and through alternative mechanisms. In agriculture, where vast areas are sprayed by diverse cocktails of antifungal resistance gains are particularly complex. Despite broad efforts, knowledge of resistance mechanisms is often limited to model genotypes and empirical evidence from the field is lacking. Here, we define and validate a high-throughput pipeline for antifungal resistance discovery informed by emerging resistance gains at continental scale. We analyzed a thousand-genome European diversity panel of the major wheat pathogen *Zymoseptoria tritici* and assessed resistance levels against over 40 fungicides covering all major classes. We optimized high-throughput phenotyping assays to comprehensively capture emerging resistance phenotypes. Pangenome-informed genotyping techniques revealed a total of 2280 genes associated with antifungal resistance. This expands by an order of magnitude the current knowledge and establishes a refined atlas of resistance mutations. We generated mutants to recapitulate several of the discovered resistance factors. Hence, our approach captures in-field resistance gains across Europe for all major fungicide classes and can define exact molecular targets. Broad knowlegde of resistance gains will guide more sustainable fungicide development pipelines.

Introduction

Fungicide resistance is a global concern for medicine and agriculture [1–5]. Critical challenges arise as the development of new fungicides is slower than the rate at of resistance emergence [6]. Understanding the molecular mechanisms of fungicide resistance is crucial to inform drug design and to mitigate resistance breakdowns and improve the lifespan of fungicides. Resistance mechanisms are typically identified through molecular genetics approaches such as random mutagenesis or reverse genetics [7–9]. However, such analyses focused on single genetic backgrounds often only poorly represent the potential for resistance mechanisms and selection in the field can produce a wider range of outcomes [10]. Variations within pathogen species in the molecular target or detoxification genes are important factors for resistance heterogeneity [11]. Genetic monitoring of pathogen populations and assessing changes in fungicide resistance can identify the rise of new resistance in the field [1,12–14]. However, targeted genetic monitoring alone is unable to pinpoint the emergence of new resistance mechanisms [5,11,15].

Genomic surveys of pathogen species enable the unbiased discovery of genetic factors contributing to trait variation including fungicide resistance [5,16,17]. Genome-wide association studies (GWAS) are powerful applications to natural populations capturing a wide spectrum of genetic factors contributing to complex traits [18]. GWAS identified standing variation in fungicide resistance in diverse crop pathogens [17,19,20]. Applications to the sugarbeet pathogen *Cercospora beticola* mapped contributions of mutations in the ergosterol biosynthesis gene *Cyp51* to azole fungicide resistance [20]. In the wheat pathogen *Zymoseptoria tritici* both the known target of azole resistance and additional not previously identified factors were mapped. GWAS discovery was facilitated by the high diversity and spatially explicit sampling [21,22]. However, the molecular basis of fungicide resistance in agricultural contexts remains largely unknown. A major factor are complex genetic contributions to resistance including *e.g.* variation generated by transposable elements (TEs) or structural variation. Such complexity was found in a regulatory region for a drug exporter gene and convergently in multiple pathogens [23–25]. Molecular targets can also evolve copy-number variation in response to fungicide selection such as the paralog emergence in *Z. tritici* and *Candida albicans* [11,26,27]. Complex genetic variation can be mapped using reference-free genotyping approaches such as k-mers integrated into GWAS [28]. Azole resistance in *Z. tritici* is at least in part governed by complex genetic variation, which was only recovered using such reference-free genotyping approaches [28].

The power of large pathogen panels to uncover variation in important traits was recently shown by the establishment of thousand-genome panels for the major wheat pathogen *Z. tritici* [5,29]. The panels revealed global patterns in pathogen emergence, adaptation to the climatic factors as well as a complex set of resistance mutations for demethylation inhibitors (DMI) such as azoles. The GWAS panel

constructed from European samples identified a total 158 genes associated with resistance to six DMIs. Notably, the panel mapped resistance to a paralog of *SdhC1*, termed *SdhC3*, which was recently discovered as a contributor to succinate dehydrogenase inhibitors (SDHI). The contribution of paralogs to fungicide resistance highlights the need to assess genetic diversity comprehensively beyond single genotypes [11,30]. The full spectrum of resistance mutations remains largely unknown as highlighted by recent work [31].

In this study, we develop and validate a high-throughput pipeline integrating the collection of a diverse pathogen panel for GWAS, a robust discovery of fungicide resistance associated genetic variants and functional validation of GWAS candidates. We determined the sensitivity of comprehensive European diversity panel of the wheat pathogen *Z. tritici* for over 40 fungicides and established a comprehensive fungicide resistance atlas cataloguing an exhaustive set of genetic factors underpinning resistance breakdowns in a geographic context.

Results

Establishment of a European diversity panel

To establish a high-throughput pipeline linking natural variation to the genetic basis of fungicide resistance, we established a five steps process depicted in (Figure 1A). The pipeline includes the establishment of a diverse strain collection capturing relevant geographic and temporal scales of fungicide resistance gains across the European continent. Second, we optimized a high-throughput phenotyping assay to profile differential fungicide susceptibility across the panel. Third, we implemented GWAS to comprehensively map genetic factors contributing to resistance across the genome and, finally, used molecular genetics assays to validate predicted resistance phenotypes. The European diversity panel captures a timespan of 15 years and originates from extensive field monitoring efforts[5]. The European continent has long experienced fungicide applications, covers a wide range of climates and fungicide regimes (Table S1). Sampling for the European diversity panel was augmented in areas of intense fungicide application and wheat production (Eurostat, 2024) (Table S2, Figure 1B). A key factor for GWAS mapping power is the diversity and size of the population [21]. To estimate the impact of collection size has on the number of genetic variants, we randomly subsampled the European diversity panel to 100-1000 strains. We found an average increase of 0.4% (1905 SNPs) per each 100 strains added, with an overall gain between 100 and 1000 of 3.7% (17141 SNPs) (Figure 1C). These results show that even a collection of 100 strains across Europe can effectively represent genetic

117 variability. The diversity panel showed an average of 1.2% synonymous point mutations and 0.4%
118 missense point mutations (Figure 1D).
119
120 **Maximize fungicide resistance discovery**
121 The composition of the GWAS panel affects mapping power [32]. To maximize locus discovery, we
122 systematically examined the effects of temporal, spatial, and panel size variation. We first subset the
123 panel into two timeframes (sampled 2005-2015 or 2016-2019 with the latter period including the first
124 applications of mefentrifluconazole. The earlier panel subset (2005-2015) consisted of 370 strains and
125 the post-2016 collection was composed of 529 strains. The post-2016 collection showed significantly
126 higher relative growth in mefentrifluconazole compared to the earlier collection ($p < 0.01$; Figure 2 A-
127 C). GWAS analyses identified five SNPs on chromosome 3 in the 2005-2015 panel, intersecting with
128 the gene 3_01019 (a Zinc-finger C2H2-type transcription factor). In contrast, the later collection set
129 revealed 152 SNPs associated with mefentrifluconazole resistance within ~41 kb of *Cyp51* and addition
130 to three SNPs located upstream of *Mfs1* (Figure 2 D).
131
132 Besides the introduction of new fungicides, fungicide application practices vary significantly across
133 Europe, leading to region-specific selection pressure. Hence, local adaptation could produce
134 heterogenous outcomes in adaptation [33]. In Europe, west-to-east represents a gradient in increased DMI
135 resistance consistent with fungicide application practices [1]. We compared 294 strains collected after
136 2015 and from either Western Europe and the British Isles or from 176 strains collected in Eastern
137 Europe (East) (Figure 2E, F, G). The relative growth of prothioconazole of strains from the two panels
138 showed no significant difference ($p < 0.2$; Figure 2E). The Western European panel revealed an amino
139 acid substitution in the *Cyp51* gene (Ser524Thr) compared to the Eastern mapping panel (Figure 2H).
140
141 Finally, we examined the influence of panel size on the statistical power of GWAS to detect fungicide
142 associations. We subset the European diversity panel into panels ranging from 100 to 800 samples, with
143 each panel size being randomized 100 times. The number of significant SNPs reached a plateau in
144 detected associations, starting at about 700 strains (Figure 3A-B). The SNPs linked to
145 mefentrifluconazole resistance converged in four different regions, including *Cyp51*, a region ~35 kb
146 from *Cyp51*, the *Mfs1* gene (for mefentrifluconazole), and 12_00117 (gene of unknown function).
147 Subsampling revealed that 200 strains were sufficient to map *Cyp51* resistance mutations (mean of 6.6
148 SNPs) and *Mfs1* (mean 4 SNPs). For prothioconazole, 200 samples were sufficient to identify *Cyp51*
149 (mean of 1.03 SNPs), and 12_00177 (mean of 8.6 SNPs). For sample sizes up to 800 strains, the
150 association mapping consistently reveals a region ~35 kb from *Cyp51*, *Cyp51* and *Mfs1*-associated
151 mutations for mefentrifluconazole (Figure 3B). Similarly, for prothioconazole, the proportion of genes
152 associated with resistance reached a plateau from 600 strains with a stable number of mutations mapped

153 in 12_00117 (3-4%) (Figure 3C). These findings show that the composition of the GWAS panel
154 significantly affects the power to map loci even under less controlled environmental conditions.
155
156 **Fungicide concentration and assay runtime impact resistance gene discovery**
157 We assessed whether fungicide concentration affects the expression of resistance mechanisms. For this,
158 we assessed growth responses to a range of epoxiconazole concentrations (10 $mg.L^{-1}$ to 0.01 $mg.L^{-1}$;
159 Figure 4A). At the lowest dose, growth of 0.2% strains was suppressed and GWAS analyses revealed
160 no significant associations for this response. Higher concentrations of epoxiconazole led to a higher
161 proportion of susceptible strains with most strains exhibiting intermediate growth levels (Figure 4B).
162 At concentrations of 0.1 and 1 $mg.L^{-1}$ epoxiconazole, GWAS mapped missense substitutions in the
163 target gene *Cyp51* including Ser524Arg and two SNPs upstream of 7_00448 (Figure 4D). At 1 $mg.L^{-1}$,
164 GWAS identified three synonymous SNPs in the drug exporter gene *Mfs1* (Figure 4E). At the highest
165 dose (10 $mg.L^{-1}$), most strains showed no growth without any GWAS associations for the observed
166 growth variation. Overall, we identified a total of 266 SNPs significantly associated with epoxiconazole
167 resistance over the concentration range. Beyond concentration, colony growth kinetics in response to
168 fungicides can potentially affect GWAS performance. Thus, we assessed GWAS outcomes for relative
169 growth 7- and 14-days post inoculation (dpi) for four different fungicides. GWAS discovery of
170 resistance mutations to the QoI azoxystrobin were unaffected by the assay runtime consistently
171 identified the Gly143Ala resistance mutation in the cytochrome b (*cob*) gene (Fig 5A). For
172 fenpropimorph (SBI class II), GWAS identified a single synonymous SNP (Pro660Pro) in the gene
173 7_00011 upstream of *Mfs1* with a 7-dpi runtime and three additional SNPs with the 14-dpi runtime.
174 Two SNPs were synonymous variants in *Mfs1* (Asn114Asn and Ile116Ile). No significant associations
175 were observed with fenhexamid (SBI class III) regardless of runtime (Fig 5BC). Finally, resistance to
176 the SDHI carboxin at the short runtime was governed by a missense mutation in a gene encoding an
177 epoxide hydrolase (1_00671; Glu115Lys) and three mutations in a gene encoding a methyltransferase
178 (8_00208). At the longer runtime, only a downstream mutation near an ABC transporter gene (4_00005)
179 was found to significantly impact resistance (Fig 5D). These findings highlight that the effects of
180 resistance mutations are expressed at least in part contingent on the degree of fungicide exposure and
181 the colony growth stage.
182
183 **Contributions of complex genetic variants**
184 Structural variation including transposable elements (TEs) and indels contribute to fungicide resistance
185 variation in *Z. tritici* [5,11,24,28]. Consequently, we genotyped the European diversity panel using a diverse
186 set of genetic markers including SNPs, short indels, k-mers, TEs, and copy number variants (CNVs).
187 We identified 8,536,499 SNPs and 6,606,877 indels segregating in the panel. For GWAS discovery, we
188 focused on the best genotyped variants and remove rare variants (minor allele frequency <5%) retaining
189 472,041 biallelic SNPs (Figure 6A). The 23,959 retained biallelic indels showed a long tail for larger

190 deletions (Table S3) (Figure 6B). We identified 186 significant indels and 901 significant SNPs. To
191 reduce the reference genome bias, we assessed k-mer frequencies among strains (Voichek and Weigel,
192 2020). We identified 66,877 significant k-mers associated to variation in fungicide resistance (Table
193 S4). We were able to localize 65.58% of the k-mers to the reference genome and a total of 98.28% to
194 the pangenome of the species (Figure 6C) (Table S5). We screen for polymorphic TE insertions in the
195 European diversity panel and identified 2,542 loci with a minor allele frequency of >1%. A total 792
196 loci showed presence of the TE in the reference genome and 1,750 were absent (Figure 6D**)**. Nearly 9%
197 of all TE polymorphisms showed a significant association with fungicide resistance (*n* = 218 loci) with
198 the *Copia* (RLC) and DNA transposons (DTX) being the most abundant TE superfamilies (Table S6).
199 Variation in copy numbers (*i.e.* CNVs) was significantly associated with fungicide resistance at 68 loci.
200 Of these, CNV loci overlapped with two genes (7_00456 and 5_00703; Table S7). Hence, reference
201 genome free genotyping and accounting for complex genetic variation improves substantially GWAS
202 discovery for resistance mutations.
203
204 **Establishment of a fungicide resistance atlas**
205 We performed and integrated GWAS findings for 15 fungicide classes relevant for agriculture. The
206 compounds including fungicides specifically recommended to combat *Z. tritici* in wheat fields,
207 additional crop protection fungicides as well as clinical compound classes such as echinocandins
208 (Figure 6A) (Table S8). We first focused on SNP-based GWAS and included 43 assessments of
209 fungicide resistance covering 30 distinct compounds, distinct assay runtimes and compound
210 concentrations. We discovered a total 901 significantly associated loci with 61.1% (*n* = 557) SNPs in
211 coding regions of 146 different genes. Of these, 41.8% (*n* = 377) SNPs were synonymous variants,
212 19.1% (*n* = 174) were missense variants and 3 were altered stop codons. The DMI class of compounds
213 (*n* = 5 tested) accounted for 71.5% of the total (645 SNPs) with 327 SNPs localized to a 40 kb region
214 near the *Cyp*51 gene encoding the molecular target of azoles. The large region with significant
215 associations is consistent with a selective sweep generating long-range linkage disequilibrium. The drug
216 exporter coding sequence of *Mfs*1 showed associations with three DMIs including cyproconazole,
217 epoxiconazole, and mefentrifluconazole. Additionally, *Mfs1* variants were associated with two
218 additional fungicide classes targeting the sterol biosynthesis pathway (*i.e.*, SBI II and SBI IV). SDHIs
219 (*n* = 4 tested) showed the second highest proportion of SNPs associated with resistance, accounting for
220 18.4 % (*n* = 166) of the significant SNPs and covered 18 genes. Isofetamid showed 143 (100%) SNPs
221 within ~10 kb of *SdhC3* gene, which encodes resistance associated paralog of the *SdhC1* subunit [11].
222 GWAS of QoI fungicides resistance identified four SNPs with azoxystrobin revealing the Gly143Ala
223 substitution in the *cytochrome b* (cob) gene encoding the molecular target of QoIs [34]. Pyribencarb
224 resistance was unexpectedly associated with substitutions in the *Cyp51* gene. GWAS for QiI fungicide
225 resistance revealed associations with a broad range of genes with florylpicoxamid resistance being
226 associated with four genes (1_01890, 3_01116, 9_00415, 11_00307) suggesting non-target site

227 resistance mechanisms. Carbamate and N-phenyl carbamate fungicide resistance were both associated
228 to the Glu198Ala substitution in the beta-tubulin gene. The substitution showed a strong negative cross-
229 resistance between the two alleles (Figure 9 A-D). In addition, the anilinopyrimidine fungicides
230 pyrimethanil and mepanipyrim also showed associations with the same Glu198Ala substitution in the
231 beta-tubulin gene. Anilinopyrimidine fungicides are thought to act on a different target, at least in *B.*
232 *cinerea* [35]. The clinically relevant echinocandin and the anilinopyrimidine fungicides not applied to
233 control *Z. tritici* revealed also significant loci in the genome (Table S8). The allele swap Glu198Ala in
234 the *beta-tubulin* gene was associated to a shift of sensitivity of the anilinopyrimidine besides to
235 carbendazim (MBC) and diethofencarb (N-phenyl carbamates). The reference free k-mer GWAS
236 approach expanded the discovery of resistance factors beyond simple variants mapped to a reference
237 genome. Assessing k-mers not mapping to the reference genome, we identified an average of 2699 k-
238 mers associated with SDHI fungicide resistance and an average of 403 k-mers for DMI resistance (Fig
239 7B). Isofetamid resistance showed the highest proportion (89.9 %) of k-mers not aligning to the
240 reference genome. The proportion of aligning k-mers increases to 76-91% when considering the
241 pangenome of the species (Table S9). For two genomes included in the species pangenome (*i.e.* 3D7
242 and 3D1) all significant k-mers mapped to the *SdhC3* paralog associated with SDHI resistance (Figure
243 7D).
244
245 **Reference-free mapping and validation of resistance factors**
246 We further investigated resistance loci for which SNP-based GWAS alone was not successful. We
247 focused on the gene *SdhC1* and carboxin resistance (Figure 8A; Table S4). The top 20 most significantly
248 associated k-mers with resistance, showed overlaps with the coding sequence of *SdhC1*. Of these k-
249 mers, 16 to a precise location pinpointing a Thr79Asn amino acid substitution (Figure 8B). The
250 substitution was missed in the SNP-based GWAS due to the very low frequency (3%) typically excluded
251 in SNP filtering (Figure 8A). The Thr79Asn was first detected in 2016 in Germany followed by a more
252 widespread occurrence across Europe with a notable frequency increase in Ireland [1]. We functionally
253 validated the impact of the Thr79Asn substitution by generating isogenic mutants in the reference
254 genome strain IPO323 lacking Ku70 (Δku70). Two independent mutants showed significantly increased
255 growth on carboxin-amended media compared to the susceptible IPO323 reference. Hence, this
256 mutation affecting the inhibitor binding site of the SDH enzyme is indeed associated with gains of
257 carboxin resistance in Europe (Scalliet et al., 2012; Steinhauer et al., 2019) (Figure 8D, Figure S1 A-
258 C).
259
260 The fungicide resistance atlas revealed a negative cross-resistance associated with the Glu198Ala
261 substitution in the beta-tubulin gene. Encoding Glu at position 198 is associated with higher resistance
262 against diethofencarb (a methyl benzimidazole carbamate class member). Encoding Ala at the same
263 position confers resistance to carbendazim (N-phenyl carbamate class) (Figure 9C) [36]. The negative

264 cross-resistance was previously characterized by showing that the Glu198Ala substitution confers
265 resistance to carbendazim and sensitivity to diethofencarb [37]. We found that Glu198Ala also mediates
266 resistance to the anilinopyrimidine fungicide class (such as pyrimethanil and mepanipyrim fungicides).
267 The anilinopyrimidine fungicides have not been used for *Z. tritici* control or for the control of wheat
268 pathogens in general. We observed a strong antagonistic growth response for strains growing either
269 well on carbendazim (10 $mg.L^{-1}$) or diethofencarb (10 $mg.L^{-1}$) (Figure 9A), as well as between
270 carbendazim (10 $mg.L^{-1}$) and pyrimethanil (50 $mg.L^{-1}$). Strains more susceptible to pyrimethanil tended
271 also to be more susceptible to diethofencarb (Figure 9BC), however the correlation in growth responses
272 was not significant ($p = 0.49$; Figure 9C). We used molecular genetics to assess the impact of the point
273 mutation associated with pyrimethanil resistance. For this, we generated isogenic lines of the IPO323
274 Δku70 background swapping the beta-tubulin Glu198 for Ala (GAG to GCG) (Figure 9D). The resulting
275 mutant (with the Glu198Ala mutation) exhibited resistance to carbendazim, and susceptibility to both
276 diethofencarb and pyrimethanil. Hence, the negative cross-resistance predicted by the fungicide
277 resistance atlas indeed replicates in functional assays.
278
279 We analyzed evidence for two additional resistance mechanisms associated with fungicide classes not
280 specifically applied against *Z. tritici.* Terbinafine, a class III sterol biosynthesis inhibitor (SBI), is
281 commonly used to treat human fungal infections and was investigated for multidrug resistance (MDR)
282 in filamentous fungi [38,39]. In *Z. tritici*, terbinafine has been used to screen for genotypes with *MFS1*
283 overexpression [25]. A recent study indicated that MDR mediated by *MFS1* promoter variation is more
284 variable than previous thought [31]. Both SNP and k-mer based GWAS identified *MFS1* as the top gene
285 associated with terbinafine resistance, with six synonymous SNPs and the most significant association
286 at position 36,492 bp on chromosome 7 (Figure 10A). Interestingly, a second *MFS* gene (10_00421)
287 was associated with terbinafine resistance through a synonymous SNP (Val531Val) and 86 mapped k-
288 mers (Figure S2 A). To test for contributions of the additional *MFS* gene to resistance, we inserted a
289 tetracyclin-repressible promoter upstream of the gene. The promoter is tunable by doxycycline. A
290 promoter swap was also performed at the *MFS1* locus as a control. In addition, we produced a knock-
291 out mutant of 10_00421 to assess whether deletion of the gene would confer oversensitivity to
292 terbinafine (Figure 10B). As expected, overexpression of *MFS1* (*OE_MFS1*) conferred resistance in
293 media supplemented with terbinafine and epoxiconazole, while doxycycline-induced repression
294 restored sensitivity (Figure 10C, Figure S2 B). However, neither overexpression nor the knock-out of
295 10_00421 altered terbinafine resistance (Figure S3 A, B). Hence, we found no support to recapitulate
296 the GWAS association in the IPO323 background. Genomic retracing of resistance alleles in the
297 European diversity panel suggested that the two resistance-associated alleles were gained independently
298 (Figure S4 A).
299

300 Finally, we focused on structural variants associated with pyrimethanil resistance. K-mer GWAS
301 identified 396 significant k-mers with 228 aligning exclusively to a genome from a strain originally
302 collection in the US (*i.e.* I93). K-mers mapped to a structural variant of 1,668 bp spanning positions
303 5,571,841-5,573,509 bp on chromosome 1 (Figure 10D). This region encodes the candidate gene
304 mediating resistance (jg.10233) and segregates both a functional and a loss-of-function haplotype in the
305 European diversity panel (Figure S5). K-mer mapping comparisons suggested additional structural
306 variation among genomes associated with resistance (Table S10) (Figure 10E). We hypothesized that
307 the truncated jg.10233 haplotype confers pyrimethanil resistance ()Figure. Introducing the alternative
308 haplotypes of jg.10233 into the IPO323 genetic background lacking the locus yielded revealed no
309 detectable variation in resistance. Hence, additional factors may play a role in this newly discovered
310 locus for pyrimethanil sensitivity.
311
312

313 **Discussion**

314

315 A comprehensive understanding of genetic factors contributing to emerging fungicide resistance is
316 crucial for effectively managing fungicide deployment and development of new compounds. This study
317 introduces a high-throughput pipeline capturing continent-wide genetic diversity of a major crop
318 pathogen. The genomic survey revealed a complex landscape of resistance against dozens of
319 compounds. Complex genetic variation makes important contributions to overall resistance. We refined
320 association mapping studies with analyses of structural variation. We confirmed some key predicted
321 resistance mutations using functional assays.

322 Sample size, genetic and phenotypic variability affect the power of GWAS analyses [21] [22,40]. The
323 established European diversity panel comprises 1420 strains sampled in a hierarchical manner. We
324 showed that even a fraction of the panel would represent a large proportion of the discovered genetic
325 diversity. However, smaller sample sizes would have prevented a robust mapping of most discovered
326 loci. Earlier population genetic analyses and monitoring programs have highlighted the heterogeneous
327 distribution of resistance across Europe [15,41]. We found direct evidence for this heterogeneity by
328 contrasting GWAS subpanels split along a East-West axis or segmenting the panel by collection years.
329 We also found that the discovery threshold to robustly discover variants was heterogenous among
330 fungicides. This is most likely explained by the population frequencies of resistance and single locus
331 contributions to resistance. The GWAS power analyses also revealed that prothioconazole resistance
332 mapped to the *cytochrome b* locus beyond the expected molecular target gene *Cyp51* and the multidrug
333 resistance factor *MFS1*. A possible explanation for the association of *cytochrome b* are the geographic
334 congruence of DMI and QoI exposure. This combination may lead to populations being co-selected for
335 dual resistance and genetic correlations. Alternatively, the multigenic basis of prothiconazole resistance
336 may either be related to yet unknown variation in DMI resistance [42] or, more likely, to the necessary
337 conversion of prothioconazole towards prothioconazole-desthio by oxidation in fungal cells, an
338 essential conversion for Cyp51 inhibition and antifungal activity [43]. Finally, we identified significant
339 impacts of the fungicide concentration in the assay on GWAS discovery. In particular, loci associated
340 with strong resistance mechanism (*e.g. Cyp51* substitutions) were detected at lower doses (sufficient to
341 control x% of the isolates) compared to complementary resistance mechanism (such as *MFS1* mediated
342 multidrug resistance). This finding suggests that in our settings, complementary resistance mechanisms
343 (*i.e.* detoxification by MFS1) display a more distinguishable phenotypic effect in backgrounds already
344 carrying primary target resistance (*i.e.* resistant *Cyp51* haplotype). The substantial improvements in
345 GWAS discovery highlights how standard fungicide resistance assay platforms can be optimized.

346 We show that a comprehensive approach to genotype genetic variation is crucial for the mapping of
347 fungicide resistance loci. The resulting fungicide resistance atlas comprises 901 significant SNPs,

348 66,877 unique K-mers, with 40,040 aligning to unique location in the reference genome, 186 significant
349 indels, 218 TE insertion polymorphisms and 68 CNV loci. The resistance atlas confirmed previously
350 discovered substitutions in *CYP51* including Ser524Thr, Ile381Val, Ser188Asn,Val136Phe and
351 Asp134Gly [44,45], Gly143Ala in *cytochrome b* [13], Glu198Ala in beta tubulin and genetic variation in or
352 nearby the multidrug resistance factor *Mfs1* [24]. Non-SNP based are known to contribute to phenotypic
353 variation including melanin production, asexual reproduction and fungicide resistance in the pathogen
354 [25,46,47]. Here, we showed that nearly a tenth of all polymorphic TE insertion loci are associated with
355 fungicide resistance. A hotspot for resistance gains mediated by TEs is in the promoter region of *Mfs1*
356 [24,25,48]. We identified previously unknown contributions by TEs (*i.e.* fluxapyroxad resistance) as well as
357 confirming the involvement of TEs for *MFS1* mediated resistance (Omrane et al., 2017). Expanding
358 genotyping approaches beyond single reference genomes was particularly important. Only ~65% of the
359 k-mers aligned to the reference genome while expanding the mapping to a pangenome resolved nearly
360 all k-mer locations [28]. K-mer based GWAS identified the dispensable *SdhC3* paralog associated with
361 increased isofetamid-resistance [11]. Hence, reference-free GWAS is an essential and powerful tool for
362 identifying standing resistance in pathogen species.

363 Functional validation through targeted manipulation of candidate genes is necessary for confirming
364 causal relationships between genetic variations and phenotypic traits. We prioritized loci identified
365 through different GWAS approaches. We confirmed the GWAS mapping of the Thr79Asn substitution
366 in the *SdhC1* gene [49]. The substitution was detected through k-mer association for carboxin resistance.
367 Furthermore, we shed light on the negative cross-resistance between mutations for anilopyrimidine
368 fungicide resistance. We found that the Glu198Ala substitution in the beta-tubulin gene confers
369 resistance to the anilopyrimidine pyrimethanil revealing a potentially species-specific effect of the
370 mutation. In *B. cinerea*, the activity of anilinopyrimidines fungicides is reversed by the addition of
371 methionine and field resistance is driven by mutations in at least two genes involved in mitochondrial
372 processes. Therefore, anilopyrimidines in *B. cinerea* are thought to primarily target a mitochondrial
373 function connected to methionine biosynthesis [35], whereas high doses affect tubulin function in *Z. tritici*.
374 We failed to replicate though the GWAS discovery of 10_00421, an MFS associated with terbinafine
375 resistance. One plausible explanation for this observation is epistasis, where the effect of one gene is
376 contingent upon the presence of specific alleles in other genes [50]. Terbinafine resistance maybe mediated
377 by 10_00421 interacting with other variants including *MFS1* overexpression. Similarly, the IPO323
378 reference genome background may not be adequate to replicate the mapped resistance effect.
379 Contributions by a structural variant associated with pyrimethanil resistance could also not be
380 replicated. Designing molecular genetic assays replicating GWAS findings are notoriously challenging
381 as associations are contingent to some degree on the genomic background and some relevant genetic
382 variation may not be accounted for. However, more efficient assay designs and the systematic screening
383 of multiple genomic backgrounds for hypothesis testing should reduce this challenge.

384 Overall, our work establishes a comprehensive fungicide resistance atlas recapitulating the emergence
385 of resistance to a multitude of fungicide classes, including most frequently used ones such as DMIs,
386 SDHIs and QoIs. The atlas provides blueprint for functionally validating contributions of individual
387 variants and maps systematically fungicide cross-resistance. We provide concrete insights how
388 pathogen diversity panels should be constructed, how to evaluate and mitigate mapping power
389 limitations, and to what extent geographic and temporal sampling is relevant. Systematic reference-free
390 genotyping accounting for complex variants turned out to be crucial to capture the full spectrum of
391 resistance gains. Building a pangenome-informed atlas of emerging resistance benefits both the
392 discovery of resistance mechanisms and guides towards more sustainable applications of compound
393 mixtures.

394

395 # Material and methods

396

397 **European diversity panel**

398 For resistance monitoring purposes, Syngenta sampled pathogens from commercial and trial sites across
399 Europe. The fungicide resistance monitoring efforts for *Z. tritici* led to a collection of 8607 strains.
400 Strains were selected from the collection based on a hierarchical clustering approach grouping sampling
401 locations into 100-km radius areas. Within each area, we balanced the collection over the 2005-2019
402 sampling years based on availability. The European diversity panel included 1420 strains from 27
403 different countries previously sequenced [5,29] (Table S1). Estimation of fungicides application were
404 based on the yearly sale in kg across the continent. The information was obtained based on the average
405 fungicide application within the time range 2011-2021 (DOI:10.2908/aei_fm_salpest09). Wheat
406 production per country was obtained by FAO and was average in tons between 2017-2019. Maps were
407 plotted in ggplot using the package ('rnaturalearth') [51,52].

408

409 **Purification of the European diversity panel**

410 All strains included in the European diversity panel were collected from infected leaves across Europe,
411 preferably with visible pycnidia, wrapped in dry paper towels, and packed into a paper envelope for
412 shipment. Upon arrival in the laboratory, samples were labeled with a unique code, and the arrival date
413 was recorded. The leaves were dried, wrapped in fresh paper towels if necessary, and stored at 4°C until
414 further processing. Leaves with symptoms were cut into 2 cm pieces, surface-sterilized in 2% bleach
415 for 2 minutes, and rinsed with sterile distilled water. Leaf cuts were placed on wet filter paper in Petri
416 dishes (1.3 mL water for 9 cm dishes) and incubated at 20°C for 24 hours. Single strains were picked
417 from cirri under a binocular microscope and transferred to V8 agar plates with antibiotics. Plates were
418 incubated for 4-7 days at 20°C. To ensure that only a single genotype was collected per sample, a single
419 spore isolation step was performed for every sample. Single colonies were subcultured on fresh V8
420 plates and incubated under the same conditions for an additional 7 days. Each isolate was stored
421 independently in a cryovial preserved in liquid nitrogen. Fresh cells harvested from V8 plates incubated
422 at 18˚C for a period of five days were used as inoculum for all experiments. Media recipes used in this
423 study have been summarized (see Table S11).

424

425 **Solid culture assays for fungicide sensitivity determination**

426 We assessed fungicide sensitivity using relative colony size estimates on solid medium (fixed fungicide
427 concentration). The European diversity panel strains stored at -80C° were arrayed in 96-well cryo-stock
428 plates in skim milk with 20% glycerol (used as mother array plates). From the mother array plates, the
429 strains to be tested were transferred using a 96-floating pin replicator tool (408FS2AS, V&P Scientific
430 Inc.) to 96-well flat bottom plates (model 3370, Corning) pre-filled with 100µl YPD liquid medium and

431 left to grow at 18°C for 7 days to reach a growth plateau. Spore suspensions were not further
432 standardized and directly spotted using a Rotor HDA (Rotor+) (Singer Inc., Watchet, UK) with sterile
433 pins (RePads) (Singer Inc., Watchet, UK) onto AE agar media plates (PlusPlates) amended or not with
434 fungicides. The fungicides were dissolved in DMSO and then mixed with AE-agar to achieve a final
435 concentration of 1% DMSO. Five different fungicide concentrations were applied to achieve final
436 concentrations of 50, 10, 1, 0.1, and 0.01 $mg.L^{-1}$ per plate. Single concentrations were then selected for
437 further GWAS studies. Control plates only contained AE-agar with 1% DMSO. Spotted AE-agar plates
438 were incubated at 20°C for 7 days in the dark before imaging. Image capture was performed using a
439 Phenobooth (Singer, Watchet, UK), and image analysis performed with the Phenosuite (version 2.21)
440 software package (Singer Inc., Watchet,) by comparing paired growth areas of colonies grown on
441 control plates without fungicide (DMSO controls) with fungicide-amended plates. The relative growth
442 area on amended media ($area_e$) relative to controls ($area_c$) was estimated using the following formula:
443

444 $$Relative\ growth = \frac{area_e - area_c}{area_c} * 100$$

445

446 Plates with signs of contamination were excluded. Plates with >2x more growth on fungicide-amended
447 plates *vs.* controls were excluded as well. Relative growth estimates and assayed fungicides are reported
448 in Table S1 and Table S2. Fungicide sensitivity of the transformants was determined on solid medium
449 (fixed fungicide concentration). For the spotting assay the suspended spores were spotted on AE media
450 amended with 1% of a 100× DMSO solution of the active ingredients to pre-melted AE-agar. AE media
451 was supplemented with 20,5,2.5 $mg.L^{-1}$ of terbinafine and epoxiconazole and each experiment was
452 performed with and without doxycycline (30 $mg.L^{-1}$). We supplemented AE media as well with 10 and
453 50 $mg.L^{-1}$ of carbendazim, 1 and 10 $mg.L^{-1}$ of diethofencarb, 20, 50 $mg.L^{-1}$ of pyrimethanil and 5,10
454 and 20 $mg.L^{-1}$ of carboxin. Pre-culture of the inoculum and fungicide sensitivity tests were performed
455 as following previously described procedures [9].
456

457 **DNA extraction, Illumina sequencing, and SNP calling**

458 Whole-genome sequencing data was previously described [5,29]. For 1134 strains high-quality genomic
459 DNA was extracted using the DNeasy Plant Mini Kits (Qiagen Inc.) following the manufacturer's
460 instructions. Paired-end sequencing of 250 cycles with an ~500 bp insert size was performed by
461 Novogene Inc. using the Illumina NovaSeq 6000 platform. We used Trimmomatic v.0.39 to trim low-
462 quality sequencing reads and remove adapter contamination in each isolate [53]. Filtered sequences were
463 aligned to the *Z. tritici* reference genome IPO323 [54] using Bowtie2 v.2.3.3 [55]. The Genome Analysis
464 Toolkit (GATK) v.4.0.1.2 [56] was used for single nucleotide polymorphism (SNP) calling and variant
465 filtration. The GATK HaplotypeCaller was run with the command -emitRefConfidence GVCF and -
466 sample_ploidy 1. Joint variant calling was performed using the tool GenotypeGVCFs merging

467 HaplotypeCaller gvcfs produced for an additional 283 from a previous study [29] with the option -maxAlt
468 2 [57]. To investigate the impact of sample size on the number of detected alleles, we randomly
469 subsampled the European collection 100 times. The number of strains included in each subsample
470 varied from 100 to 1000. Vcftools v0.1.15 [58] was used to perform the random subsetting. To estimate
471 the total number of SNPs based on the annotation of the *Z. tritici* 2015 genome [59], we used SnpEFF [60]
472 with the "-csvStats". Finally, the total number of synonymous and missense point mutations was
473 normalized based on the corresponding gene length (see Table S12).
474
475 **SNP-based genome-wide association mapping and bootstrapping**
476 For SNP-based GWAS on the Europe diversity panel, we retained SNPs with a genotyping call rate of
477 ≥90% and a MAF ≥5% resulting in a final set of 472,103 biallelic SNPs (Table S1). Traits for GWAS
478 included the relative growth estimates for 43 traits (Table S2). We tested 15 fungicide classes with an
479 over representation of DMI, SDHI, QOI, QII, classes applied in *Z. tritici.* We accounted for relatedness
480 by constructing a genetic relatedness matrix (GRM) among strains using all genome-wide SNPs with
481 the option "-gk 2" in Gemma [61]. Thus, all the associations were performed using a univariate linear
482 mixed model (MLM+K) where K is the GRM as a random effect:

483 $$y = Wa + x\beta + u + \varepsilon; u \sim MVN_n(0, \lambda\tau^{-1}K), \varepsilon \sim MVN_n(0, \tau^{-1}I_n)$$

484 y represents a vector of phenotypic values for n individuals; W is a matrix of covariates (fixed effects
485 with a column vector of 1), α is a vector of the corresponding coefficients, including the intercept; x is
486 a vector of the genotypes of the SNP marker, β is the effect size of the marker; u is a vector of random
487 individual effects; ε is a vector of random error; τ-1 is the variance of the residual errors; λ is the ratio
488 between the two variance components; K is the $n \times n$ GRM and I_n is an $n \times n$ identity matrix and MVN_n
489 represents the multivariate normal distribution. We applied a stringent Bonferroni threshold ($\alpha = 0.05$;
490 $p = \alpha$ / total number of SNPs) to identify most robust SNP associations. Significant SNPs were annotated
491 using snpEff v5.0e [60]. We provide links to all association mapping outcomes in Table S13. To
492 investigate the impact of geographic and temporal distribution on the number of detected resistant
493 alleles, the European diversity panel was split in strains collected from the West and East of Europe
494 after 2016. For the temporal distribution, we split the strains before and after 2016. T-test between
495 relative growth values of West and East and before-after 2016 strains were performed using the
496 command t.test built-in function in R. Subsequently, the results were visualized through figures
497 generated in R ggplot2 and adjusted in Illustrator [52]. In the Manhattan plot for p-value within 0.1 and
498 0.01 we retained only 1 out of every 30 rows, for p-value within than 0.2 and 0.1 we retained only 1 out
499 of every 300 rows and for p-value greater than 0.2 we retained only 1 out of every 400 rows for
500 visualization purposes. To investigate the impact of sample size on the number of detected resistant
501 alleles, the number of strains included in each subsample varied from 100 to 800 strains. Vcftools

502 v0.1.15 [58] and gemma were used to perform the random subsetting and the GWAS. SNPEFF [60] was
503 utilized to annotate the SNPs and genes based on the *Z. tritici* 2015 genome annotation [59] (See Table
504 S14 and Table S15).

505 **K-mer based genome-wide association mapping**

506 We performed k-mer based GWAS on the same 43 traits used for SNP-based GWAS following a
507 previously described approach [62]. We used k-mers of 25-bp length as suggested for small genomes such
508 as *Z. tritici* following previous studies [28]. Quality-filtered sequencing reads (see above) of 1406 strains
509 from the European diversity panel were used for k-mer screening. K-mers were counted using a two-
510 step process: The canonization involved treating each k-mer and its reverse complement as equivalent.
511 In contrast, non-canonization treats the k-mer and its reverse complement as distinct entities. A k-mer
512 and the reverse complement are supposed to have the same chance to appear in fastq files. However,
513 bias can favor the presence of one of the two forms for some k-mer. Therefore, k-mers were then filtered
514 based on two criteria: (1) a k-mer must appear in both its canonized and non-canonized forms in at least
515 5% of the strains, and (2) it must appear in both forms in at least 20% of the strains in which it was
516 found. A GRM was estimated with EMMA (Efficient Mixed-Model Association) as an identity-by-state
517 (IBS) matrix under the assumption that each k-mer has a small, random effect on the phenotype. GWAS
518 was performed by using an LMM+K model in Gemma with a likelihood ratio test to determine p-values.
519 Beta estimation and significance testing were performed using the patched version of kmers_gwas.py,
520 incorporating the recommendations outlined (https://github.com/voichek/kmersGWAS/issues/53 and
521 https://github.com/voichek/kmersGWAS/issues/91). A k-mer was significant when the p-value passed
522 the permutation-based threshold as described by Voichek and Weigel (2020). For all k-mer association
523 mapping see Table S16. We attempted to map all significant k-mers for each trait to the reference
524 genome using the short-read aligner bowtie v1.2.2 [55] with the command "-a --best --strata" and retained
525 the k-mers with a unique alignment (see Table S4). We used the center position of the mapped k-mer
526 to the reference genome as a coordinate to inspect nearby features using BEDtools v2.31.0 [63]. Finally,
527 the proportion of significant k-mers aligning and not aligning across the 19 pangenomes [30], per each
528 fungicide, was obtained with bowtie v1.2.2, with the command "-a –best –strata" (Langmead and
529 Salzberg, 568 2012) (see Table S9). The proportion of significant k-mers aligning and not aligning to
530 I93, UA005, I93 jg.10233 and SV_UA005.jg.10233 regions were obtained with bowtie v1.2.2, with the
531 command "-a –best –strata". We provided each k-mer association mapping file (see Table S13).
532

533 **TEs detection and association study**

534 We performed TE based GWAS on the same 43 traits used for SNP-based GWAS. TE annotation was
535 performed with ngs-te-mapper2 [64]. This is a three-stage pipeline. In the first stage the sequencing reads
536 are queried against a library of TE sequences, for which we used the TE consensus sequences obtained
537 from 20 fully assembled genomes of 19 global strains [30]. The "junction reads" that align both on a TE

538 consensus sequence and on the flanking, genome are used to determine the site of insertion of reference
539 and non-reference TEs. Non reference TEs were categorized as reference TEs when located within
540 proximity (up to 100 bp) to a reference TE of the same family. This adjustment aimed to mitigate
541 potential inaccuracies in detection while enhancing the overall frequency of detected TEs.
542 Consequently, insertions of the identical element within a narrow window were treated as a singular
543 insertion for subsequent analyses. For the association analysis, we set the maf to 1% and we used the
544 relatedness matrix (GRM) estimated from european vcf the genome-wide SNPs using the option "-gk
545 2" in GEMMA [61]. A summary of the significant TEs is in Table S6. We provided each TE association
546 mapping file (see Table S13).
547
548 **CNV genotyping**
549 We performed CNV-based GWAS on the same 43 traits used for SNP-based GWAS. We trimmed the
550 Illumina raw reads with Trimmomatic v.0.32 [53] and mapped to the *Z. tritici* (IPO323) reference genome
551 with Bowtie2 v.2.4.0 very-sensitive-local option. To define copy number variation (CNV) to the dataset
552 (n=1420 samples) we used GATK germline copy number caller v.4.1.9.0[56] in case mode against a
553 previously constructed GATK CNV cohort model built from 1109 *Z. tritici* genomes[65]. CNV interval
554 was set to 1000 bp windows with no overlap. We filtered for GC content in windows (min=0.1 and
555 max=0.9), as well as extremely low and high read counts (--low-count-filter-count-threshold = 5, --
556 extreme-count-filter-minimum-percentile = 1, --extreme-count-filter-maximum-percentile=99). We
557 used a prior table for chromosomal ploidy to assign prior probabilities for each ploidystate. Finally, we
558 called CNV genotypes using the Determine Germline Contig Ploidy, Germline CNV Caller and Post
559 process Germline CNV Calls functions in case mode. CNV GWAS analysis involved preprocessing the
560 data by removing duplicated chromosomes, converting CNV events into four categories (more than one
561 copy, one copy, no copy, or missing), and identifying and removing the least frequent allele at each
562 position, retaining only the most frequent allele. The association analysis was conducted using
563 GEMMA [61] with a minor allele frequency threshold of 5% and with GRM constructed from genome-
564 wide SNPs using the "-gk 2" option. A summary of the significant CNVs is in Table S7. We provided
565 each CNV association mapping file (see Table S13).
566
567 **Indels-based genome-wide association mapping**
568 For Indels-based GWAS on the Europe diversity panel, we retained Indels with a genotyping call rate
569 of ≥90% and a MAF ≥5% resulting in a final set of 23,959 indels. Traits for GWAS included the relative
570 growth estimates for 43 traits (Table S2). We tested 15 fungicide classes with an over-representation of
571 DMI, SDHI, QOI, QII, classes applied in *Z. tritici.* We accounted for relatedness by constructing a
572 genetic relatedness matrix (GRM) among strains using all genome-wide SNPs with the option "-gk 2"
573 in GEMMA [61]. Thus, all the associations were performed using a univariate linear mixed model

574 (MLM+K), where K is the GRM as a random effect. A summary of the significant Indels is in (Table
575 S17). We provided each Indels association mapping file (see Table S13).
576
577 **Mutant selection criteria**
578 Locus refinement was conducted employing stringent selection criteria encompassing *p*-value
579 significance, effect size, gene functionality, and mutation type (intragenic vs. intergenic). The
580 significance threshold for the *p*-value was determined by adhering to Bonferroni's correction.
581 Additionally, we focused on selecting mutations with a beta (>=2), indicative of a twofold effect.
582 Missense point mutations were accorded higher priority over synonymous mutations. Moreover,
583 emphasis was placed on previously characterized functions, such as MFS, and SDH subunits, while
584 structural variants were given preferential consideration. The list of the mutants is in Table S18.
585
586 **Molecular methods for transformations**
587 All the genes were synthesized by GENEWIZ (Suzhou, China) and were inserted in the multisite
588 pNOV2114 Hyg_gateway. To generate the KO of 10_00421 (KO_ Zt09_10_00421), we designed the
589 final plasmid Hygr_pNOV2114_KO_G10877_MFS. The pNOV2114 backbone was supplemented
590 with a region 799bps upstream the 5' of 10_00421 gene and 2274 downstream 3' of the 10_00421 gene.
591 We substitute the 10_00421 gene with a short terminator, followed by the constitutive promoter TrpC
592 [66] , and with the hygromycin resistance cassette (see Figure 10B for a graphical overview and
593 supplemental file Table S18 with plasmids sequences). For the structural variants SV_I93.jg.10233 and
594 SV_UA005.jg.10233 we inserted in the IPO323 background with a region of 1560 bps at position
595 5571672 on chromosome 1. The flanking region included 977 bps upstream and 1000 bps downstream,
596 the position 5571672 on chromosome 1. The Hygr_pNOV2114_jg10233_I93 and
597 Hygr_pNOV2114_jg10233_UA005 included a short terminator, followed by the constitutive promoter
598 TrpC [66], followed by the hygromycin resistance cassette and, respectively the structural variants of I93
599 (1556 bps) and of UA005 (1560 bps). For generating the expression constructs under the control of a
600 tetracycline-repressing promoter we designed a fragment containing the full Tet repressor expression
601 cassette followed by operator sequences fused to mfaI minimal promoter upstream the starting codon
602 of *Mfs1* (Hygr_pNOV2114_OE_G07914.1_MFS1) and 09_00421
603 (Hygr_pNOV2114_OE_G10877_newMfs). For the Single swap (SW) point mutation we selected a
604 region of 1888 bps encompassing the *beta-tubulin* (pNOV2114_SW_G02218_BetaTUB) gene and a
605 region of 2017 bps encompassing the *SdhC1* gene (pNOV2114_SW_G09103_SDHC). All entry and
606 subsequent binary plasmids were transfer to *A. tumefaciens*. *Z. tritici* transformation was performed as
607 described previously [5,67]. *Z. tritici* transformants were selected on Hygromycine, Carbendazim (AE +
608 10 $mg.L^{-1}$) or Carboxin (AE + 10 $mg.L^{-1}$) depending by the selection cassette. All clones were then
609 validated by PCR and three combination of primers were tested (Table S19). For the single-point
610 mutation, a Sanger sequencing step was included to confirm the cloned fragment.

611
612 **AlphaFold2**
613 We further investigated the 3D structure of SDHC1 using AlphaFold2 [68]. We imputed the sequences
614 SDHC1 (08_00228) to predict the 3D structure. Local Distance Difference Test (lDDT) scores were
615 employed to assess the confidence in amino acid positioning within their local structural environments.
616 While the first few amino acids generally exhibit lower lDDT scores, the score at position 79 was high
617 (approximately 100), indicating a high degree of confidence in its predicted location. However, it's
618 important to acknowledge that the lDDT score at this position could be influenced by the low coverage
619 of SDHC1 sequences, particularly at the beginning of the protein, within the AlphaFold2 database.
620
621
622 **Declarations**
623
624 **Acknowledgements**: We thank Nadja Lindenberger, Regula Frey, Salvatore Accardo and Syngenta's
625 monitoring team for collecting the strains analyzed in this work. Ursula O provided insightful
626 feedback on the manuscript.
627
628 **Funding**: This work was supported by an Innosuisse grant (32532.1 IP-LS) to GS and DC. DC was
629 supported by Swiss National Science Foundation grants 173265 and 201149.
630
631 **Competing interests**: CD, DE, DF, SFFT and GS were employed by Syngenta at the time of the
632 study. The other authors declare no conflict of interest exists.
633
634 **Data availability**: Genome sequencing data is available on the NCBI Sequence Read Archive
635 (accession numbers are provided in Supplementary Table S1). Additional datasets are made available
636 in supplementary materials.
637

References

1. Hellin, P. *et al.* Spatio-temporal distribution of DMI and SDHI fungicide resistance of *ZYMOSEPTORIA TRITICI* throughout EUROPE based on frequencies of key target-site alterations. *Pest Manag. Sci.* **77**, 5576–5588 (2021).
2. Lockhart, S. R., Chowdhary, A. & Gold, J. A. W. The rapid emergence of antifungal-resistant human-pathogenic fungi. *Nat. Rev. Microbiol.* **21**, 818–832 (2023).
3. Schürch, S. *et al.* Occurrence of *Aspergillus fumigatus* azole resistance in soils from Switzerland. *Med. Mycol.* **61**, myad110 (2023).
4. Zhang, Y.-Z. *et al.* Genetic diversity of field Fusarium asiaticum and Fusarium graminearum isolates increases the risk of fungicide resistance. *Phytopathol. Res.* **5**, 51 (2023).
5. Puccetti, G. *et al.* A large European diversity panel reveals complex azole fungicide resistance gains of a major wheat pathogen. Preprint at https://doi.org/10.1101/2025.03.19.644200 (2025).
6. Fisher, M. C., Hawkins, N. J., Sanglard, D. & Gurr, S. J. Worldwide emergence of resistance to antifungal drugs challenges human health and food security. *Science* **360**, 739–742 (2018).
7. Fouché, G. *et al.* Directed evolution predicts cytochrome *b* G37V target site modification as probable adaptive mechanism towards the QII fungicide fenpicoxamid in *Zymoseptoria tritici*. *Environ. Microbiol.* **24**, 1117–1132 (2022).
8. Rubin, A. E. *et al.* EMS and UV irradiation induce unstable resistance against CAA fungicides in Bremia lactucae. *Eur. J. Plant Pathol.* **129**, 339–351 (2011).
9. Scalliet, G. *et al.* Mutagenesis and Functional Studies with Succinate Dehydrogenase Inhibitors in the Wheat Pathogen Mycosphaerella graminicola. *PLoS ONE* **7**, e35429 (2012).
10. Kretschmer, M. *et al.* Fungicide-Driven Evolution and Molecular Basis of Multidrug Resistance in Field Populations of the Grey Mould Fungus Botrytis cinerea. *PLoS Pathog.* **5**, e1000696 (2009).
11. Steinhauer, D. *et al.* A dispensable paralog of succinate dehydrogenase subunit C mediates standing resistance towards a subclass of SDHI fungicides in Zymoseptoria tritici. *PLOS Pathog.* **15**, e1007780 (2019).
12. Bellah, H. *et al.* A highly multiplexed assay to monitor pathogenicity, fungicide resistance and gene flow in the fungal wheat pathogen Zymoseptoria tritici. *PLOS ONE* **18**, e0281181 (2023).
13. Torriani, S. F., Brunner, P. C., McDonald, B. A. & Sierotzki, H. QoI resistance emerged independently at least 4 times in European populations of *Mycosphaerella graminicola*: Qol resistance in *Mycosphaerella graminicola*. *Pest Manag. Sci.* **65**, 155–162 (2009).
14. Torriani, S. F. F. *et al.* Zymoseptoria tritici: A major threat to wheat production, integrated approaches to control. *Fungal Genet. Biol.* **79**, 8–12 (2015).
15. Cools, H. J. & Hammond-Kosack, K. E. Exploitation of genomics in fungicide research: current status and future perspectives: Genomics and fungicide research. *Mol. Plant Pathol.* **14**, 197–210 (2013).

16. He, X. *et al.* Genomic diversity of the pathogenic fungus Aspergillus fumigatus in Japan reveals the complex genomic basis of azole resistance. *Commun. Biol.* **7**, 274 (2024).
17. Pereira, D., McDonald, B. A. & Croll, D. The Genetic Architecture of Emerging Fungicide Resistance in Populations of a Global Wheat Pathogen. *Genome Biol. Evol.* **12**, 2231–2244 (2020).
18. Bartoli, C. & Roux, F. Genome-Wide Association Studies In Plant Pathosystems: Toward an Ecological Genomics Approach. *Front. Plant Sci.* **8**, 763 (2017).
19. Hartmann, F. E. *et al.* The complex genomic basis of rapid convergent adaptation to pesticides across continents in a fungal plant pathogen. *Mol. Ecol.* **30**, 5390–5405 (2021).
20. Spanner, R. *et al.* Genome-Wide Association and Selective Sweep Studies Reveal the Complex Genetic Architecture of DMI Fungicide Resistance in *Cercospora beticola*. *Genome Biol. Evol.* **13**, evab209 (2021).
21. Hayes, B. Overview of Statistical Methods for Genome-Wide Association Studies (GWAS). in *Genome-Wide Association Studies and Genomic Prediction* (eds Gondro, C., Van Der Werf, J. & Hayes, B.) vol. 1019 149–169 (Humana Press, Totowa, NJ, 2013).
22. Sánchez-Vallet, A., Hartmann, F. E., Marcel, T. C. & Croll, D. Nature's genetic screens: using genome-wide association studies for effector discovery: Nature's genetic screens. *Mol. Plant Pathol.* **19**, 3–6 (2018).
23. Chen, F. *et al.* Fungicide-induced transposon movement in Monilinia fructicola. *Fungal Genet. Biol.* **85**, 38–44 (2015).
24. Omrane, S. *et al.* Fungicide efflux and the MgMFS1 transporter contribute to the multidrug resistance phenotype in *Z ymoseptoria tritici* field isolates: Fungicide efflux & *MgMFS 1* contribute to MDR in *Z. tritici*. *Environ. Microbiol.* **17**, 2805–2823 (2015).
25. Omrane, S. *et al.* Plasticity of the *MFS1* Promoter Leads to Multidrug Resistance in the Wheat Pathogen *Zymoseptoria tritici*. *mSphere* **2**, (2017).
26. Hawkins, N. J. *et al.* Paralog Re-Emergence: A Novel, Historically Contingent Mechanism in the Evolution of Antimicrobial Resistance. *Mol. Biol. Evol.* **31**, 1793–1802 (2014).
27. Sanglard, D. Finding the needle in a haystack: Mapping antifungal drug resistance in fungal pathogen by genomic approaches. *PLOS Pathog.* **15**, e1007478 (2019).
28. Dutta, A., McDonald, B. A. & Croll, D. *Combined Reference-Free and Multi-Reference Approaches Uncover Cryptic Variation Underlying Rapid Adaptation in Microbial Pathogens*. http://biorxiv.org/lookup/doi/10.1101/2022.05.16.492091 (2022) doi:10.1101/2022.05.16.492091.
29. Feurtey, A. *et al.* A thousand-genome panel retraces the global spread and adaptation of a major fungal crop pathogen. *Nat. Commun.* **14**, 1059 (2023).
30. Badet, T., Oggenfuss, U., Abraham, L., McDonald, B. A. & Croll, D. A 19-isolate reference-quality global pangenome for the fungal wheat pathogen Zymoseptoria tritici. *BMC Biol.* **18**, 12 (2020).
31. Neau, E., Patry-Leclaire, S., Duplaix, C., Walker, A.-S. & Fillinger, S. Screen of potential multi-drug resistant Zymoseptoria tritici field isolates reveals genotypic and phenotypic diversity suggesting multiple mechanisms involved in MDR. in *16 TH EUROPEAN CONFERENCE ON FUNGAL GENETICS* (Susanne Zeilinger-Migsich and Hubertus Haas, Innsbruck,, Austria, 2023).

32. Peterson, R. E. *et al.* Genome-wide Association Studies in Ancestrally Diverse Populations: Opportunities, Methods, Pitfalls, and Recommendations. *Cell* **179**, 589–603 (2019).
33. Pimentão, A. R., Cuco, A. P., Pascoal, C., Cássio, F. & Castro, B. B. Current trends and mismatches on fungicide use and assessment of the ecological effects in freshwater ecosystems. *Environ. Pollut.* **347**, 123678 (2024).
34. Fraaije, B. A. *et al.* Role of Ascospores in Further Spread of QoI-Resistant Cytochrome *b* Alleles (G143A) in Field Populations of *Mycosphaerella graminicola*. *Phytopathology®* **95**, 933–941 (2005).
35. Mosbach, A. *et al.* Anilinopyrimidine Resistance in Botrytis cinerea Is Linked to Mitochondrial Function. *Front. Microbiol.* **8**, 2361 (2017).
36. Hawkins, N. J. & Fraaije, B. A. Fitness Penalties in the Evolution of Fungicide Resistance. *Annu. Rev. Phytopathol.* **56**, 339–360 (2018).
37. Liu, S., Che, Z. & Chen, G. Multiple-fungicide resistance to carbendazim, diethofencarb, procymidone, and pyrimethanil in field isolates of Botrytis cinerea from tomato in Henan Province, China. *Crop Prot.* **84**, 56–61 (2016).
38. Leroux, P., Chapeland, F., Desbrosses, D. & Gredt, M. Patterns of cross-resistance to fungicides in Botryotinia fuckeliana (Botrytis cinerea) isolates from French vineyards. *Crop Prot.* **18**, 687–697 (1999).
39. Moreno-Sabater, A. *et al.* Terbinafine Resistance in Dermatophytes: A French Multicenter Prospective Study. *J. Fungi* **8**, 220 (2022).
40. Drenth, A., McTaggart, A. R. & Wingfield, B. D. Fungal clones win the battle, but recombination wins the war. *IMA Fungus* **10**, 18 (2019).
41. Feurtey, A. *et al. A Thousand-Genome Panel Retraces the Global Spread and Climatic Adaptation of a Major Crop Pathogen*. http://biorxiv.org/lookup/doi/10.1101/2022.08.26.505378 (2022) doi:10.1101/2022.08.26.505378.
42. Parker, J. E. *et al.* Mechanism of Binding of Prothioconazole to *Mycosphaerella graminicola* CYP51 Differs from That of Other Azole Antifungals. *Appl. Environ. Microbiol.* **77**, 1460–1465 (2011).
43. Parker, J. E. *et al.* Prothioconazole and Prothioconazole-Desthio Activities against Candida albicans Sterol 14-α-Demethylase. *Appl. Environ. Microbiol.* **79**, 1639–1645 (2013).
44. Cools, H. J. *et al.* Impact of Recently Emerged Sterol 14α-Demethylase (CYP51) Variants of Mycosphaerella graminicola on Azole Fungicide Sensitivity. *Appl. Environ. Microbiol.* **77**, 3830–3837 (2011).
45. Leroux, P., Albertini, C., Gautier, A., Gredt, M. & Walker, A.-S. Mutations in theCYP51 gene correlated with changes in sensitivity to sterol 14α-demethylation inhibitors in field isolates ofMycosphaerella graminicola. *Pest Manag. Sci.* **63**, 688–698 (2007).
46. Krishnan, P. *et al.* Transposable element insertions shape gene regulation and melanin production in a fungal pathogen of wheat. *BMC Biol.* **16**, 78 (2018).
47. Wang, C., Milgate, A. W., Solomon, P. S. & McDonald, M. C. The identification of a transposon affecting the asexual reproduction of the wheat pathogen *Zymoseptoria tritici*. *Mol. Plant Pathol.* **22**, 800–816 (2021).

769 48. Patry-Leclaire, S., Neau, E., Pitarch, A., Walker, A.-S. & Fillinger, S. Plasticity of the
770 MFS1 promotor is not the only driver of Multidrug resistance in Zymoseptoria tritici.
771 Preprint at https://doi.org/10.1101/2023.12.27.573052 (2023).
772 49. Rehfus, A., Strobel, D., Bryson, R. & Stammler, G. Mutations in *sdh* genes in field
773 isolates of *Zymoseptoria tritici* and impact on the sensitivity to various succinate
774 dehydrogenase inhibitors. *Plant Pathol.* **67**, 175–180 (2018).
775 50. Campa, A., García-Fernández, C. & Ferreira, J. J. Genome-Wide Association Study
776 (GWAS) for Resistance to Sclerotinia sclerotiorum in Common Bean. *Genes* **11**, 1496
777 (2020).
778 51. Massicotte, P. & South, A. rnaturalearth: World Map Data from Natural Earth. 1.0.1
779 https://doi.org/10.32614/CRAN.package.rnaturalearth (2017).
780 52. Wickham, H. *et al.* ggplot2: Create Elegant Data Visualisations Using the Grammar of
781 Graphics. 3.5.1 https://doi.org/10.32614/CRAN.package.ggplot2 (2007).
782 53. Bolger, A. M., Lohse, M. & Usadel, B. Trimmomatic: a flexible trimmer for Illumina
783 sequence data. *Bioinformatics* **30**, 2114–2120 (2014).
784 54. Goodwin, S. B. *et al.* Finished Genome of the Fungal Wheat Pathogen Mycosphaerella
785 graminicola Reveals Dispensome Structure, Chromosome Plasticity, and Stealth
786 Pathogenesis. *PLoS Genet.* **7**, e1002070 (2011).
787 55. Langmead, B. & Salzberg, S. L. Fast gapped-read alignment with Bowtie 2. *Nat. Methods*
788 **9**, 357–359 (2012).
789 56. McKenna, A. *et al.* The Genome Analysis Toolkit: A MapReduce framework for
790 analyzing next-generation DNA sequencing data. *Genome Res.* **20**, 1297–1303 (2010).
791 57. Auwera, G. van der & O'Connor, B. D. *Genomics in the Cloud: Using Docker, GATK,*
792 *and WDL in Terra*. (O'Reilly Media, Sebastopol, CA, 2020).
793 58. Danecek, P. *et al.* The variant call format and VCFtools. *Bioinformatics* **27**, 2156–2158
794 (2011).
795 59. Grandaubert, J., Bhattacharyya, A. & Stukenbrock, E. H. RNA-seq-Based Gene
796 Annotation and Comparative Genomics of Four Fungal Grass Pathogens in the Genus
797 *Zymoseptoria* Identify Novel Orphan Genes and Species-Specific Invasions of
798 Transposable Elements. *G3 GenesGenomesGenetics* **5**, 1323–1333 (2015).
799 60. Cingolani, P. *et al.* A program for annotating and predicting the effects of single
800 nucleotide polymorphisms, SnpEff: SNPs in the genome of Drosophila melanogaster
801 strain w ^{1118} ; iso-2; iso-3. *Fly (Austin)* **6**, 80–92 (2012).
802 61. Zhou, X. & Stephens, M. Genome-wide efficient mixed-model analysis for association
803 studies. *Nat. Genet.* **44**, 821–824 (2012).
804 62. Voichek, Y. & Weigel, D. Identifying genetic variants underlying phenotypic variation in
805 plants without complete genomes. *Nat. Genet.* **52**, 534–540 (2020).
806 63. Quinlan, A. R. & Hall, I. M. BEDTools: a flexible suite of utilities for comparing
807 genomic features. *Bioinformatics* **26**, 841–842 (2010).
808 64. Linheiro, R. S. & Bergman, C. M. Whole Genome Resequencing Reveals Natural Target
809 Site Preferences of Transposable Elements in Drosophila melanogaster. *PLoS ONE* **7**,
810 e30008 (2012).

65. Tralamazza, S. M., Gluck-Thaler, E., Feurtey, A. & Croll, D. Copy number variation introduced by a massive mobile element facilitates global thermal adaptation in a fungal wheat pathogen. *Nat. Commun.* **15**, 5728 (2024).
66. Derbyshire, M. C. *et al.* Phosphopantetheinyl transferase (Ppt)-mediated biosynthesis of lysine, but not siderophores or DHN melanin, is required for virulence of Zymoseptoria tritici on wheat. *Sci. Rep.* **8**, 17069 (2018).
67. Bowler, J. *et al.* New capabilities for *Mycosphaerella graminicola* research. *Mol. Plant Pathol.* **11**, 691–704 (2010).
68. Mirdita, M. *et al.* ColabFold: making protein folding accessible to all. *Nat. Methods* **19**, 679–682 (2022).

822 **Figures**
823

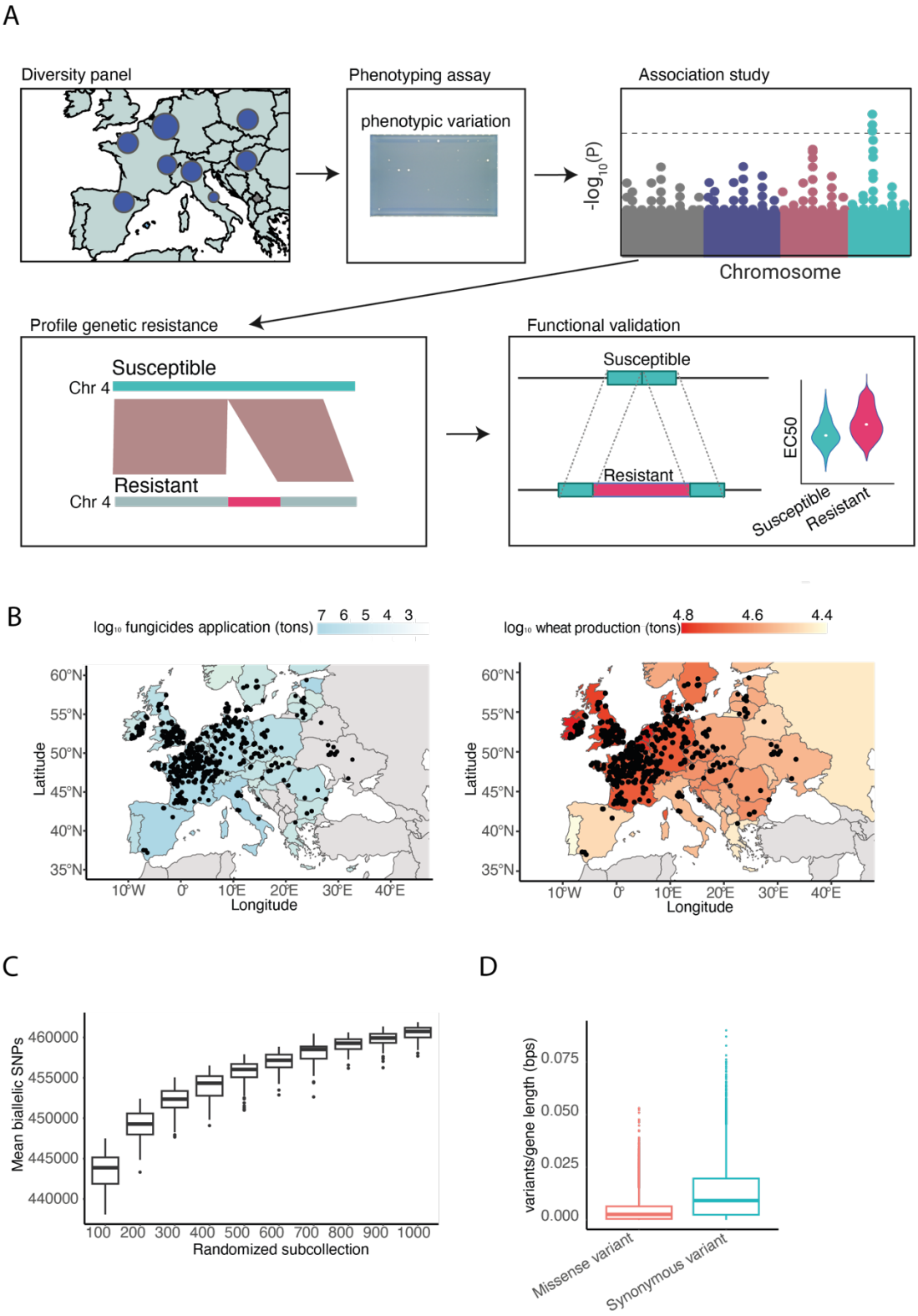

824
825
826 **Figure 1. Flowchart of the fungicide resistance discovery pipeline connecting natural variation to**
827 **the genetic basis of resistance**. A: Establishing a comprehensive collection of strains across space and
828 time, designing and optimizing a phenotypic assay to profile fungicide resistance, performing GWAS,
829 and conducting functional validation. B-C: European maps representing European isolate distribution
830 (black dots) and colored the average ton of fungicide applied between 2011 and 2020 and wheat

production in between 2017 and 2019. C: Average number of SNP variants derived from a random subsampling of the European collection from 100 up to 1000 strains. D: Percentage of synonymous and missense variants, normalized by gene length across the core chromosomes in the European collection.

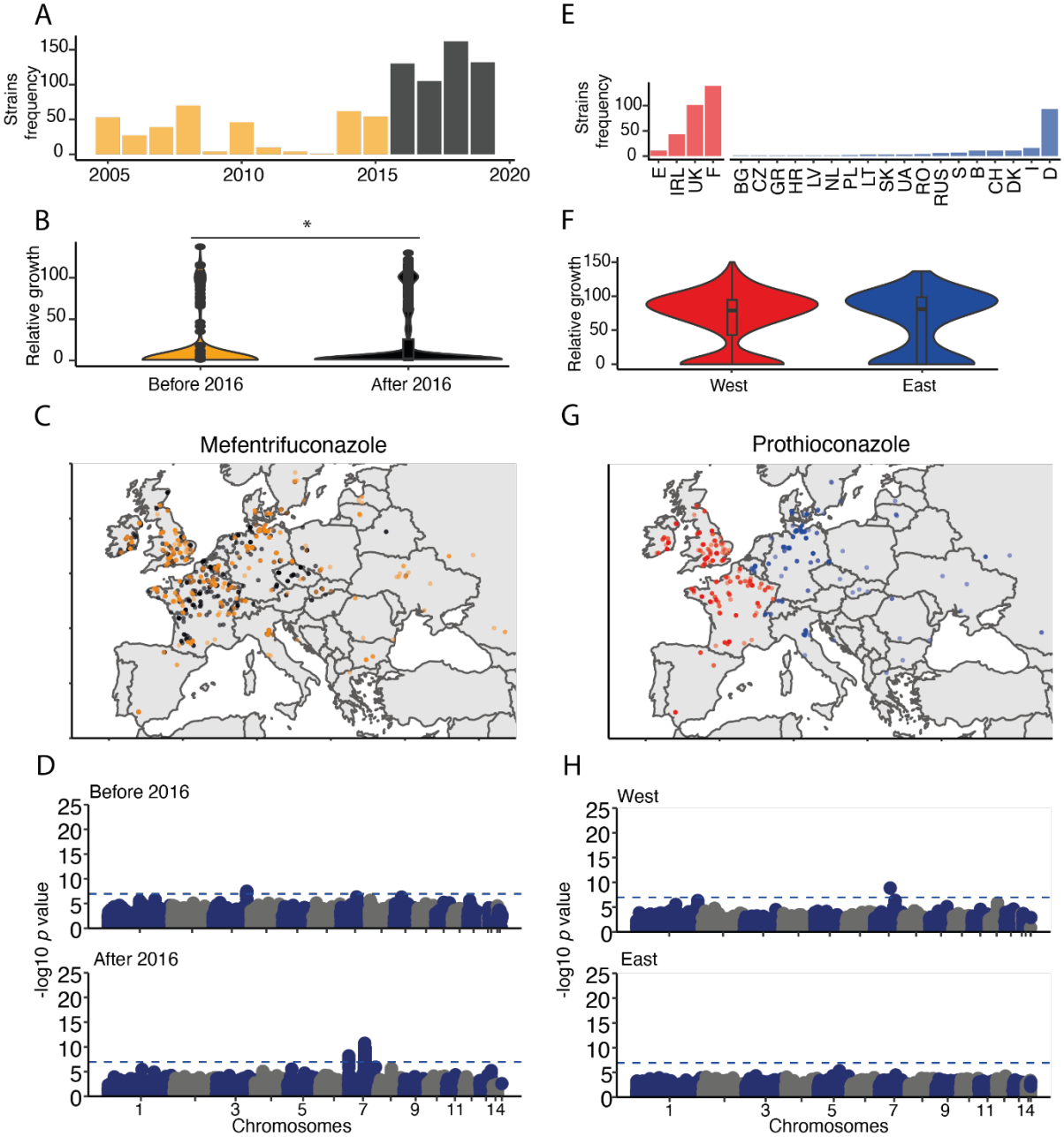

Figure 2. Sampling distribution and association studies of geographically and sampling epoch-constrained panels. (A) Frequency of strains before and after 2015 per year. (B) Relative growth differences for mefentrifluconazole (7 dpi, 0.1 mg.L^{-1}) * t-test p-value<0.05. (C) Geographic distribution of strains before and after 2015. (D) Manhattan plot of mefentrifluconazole resistance based on relative growth. For visualization purposes, SNPs have been randomly subsampled. (E) Frequency of strains in the West and East of Europe. (F) Relative growth differences for prothioconazole (7 dpi, 1 mg.L^{-1}). (G) Geographic distribution of strains in Western and Eastern Europe. (H) Manhattan plot of prothioconazole resistance based on relative growth values.

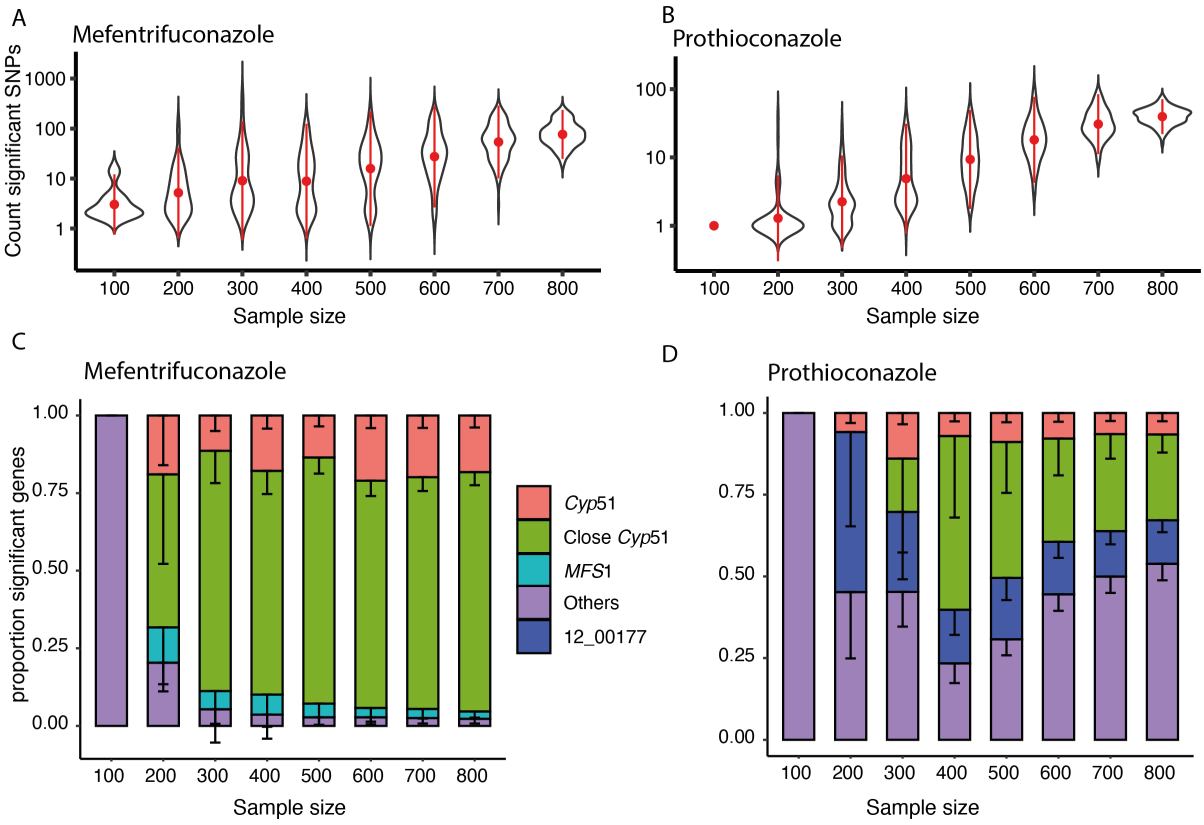

Figure 3. Significant associations (Bonferroni) based on random subsets of strains assayed for mefentrifluconazole and prothiconazole resistance. (A-B) The average number of associations above the Bonferroni threshold for various subsample sizes, bootstrapped 100 times. Summaries are based on relative growth values for mefentrifluconazole and prothiconazole. (C-D): Significant association counts for associations in proximity to genes with known functions. Color coding indicates the functional class of the closest gene: purple (*Cyp51*), green (others), pink (close to *Cyp51* – from 7_00451 to 7_00459), light blue (MFS1), red (*Cytb*), light green (others), light green (12_00177).

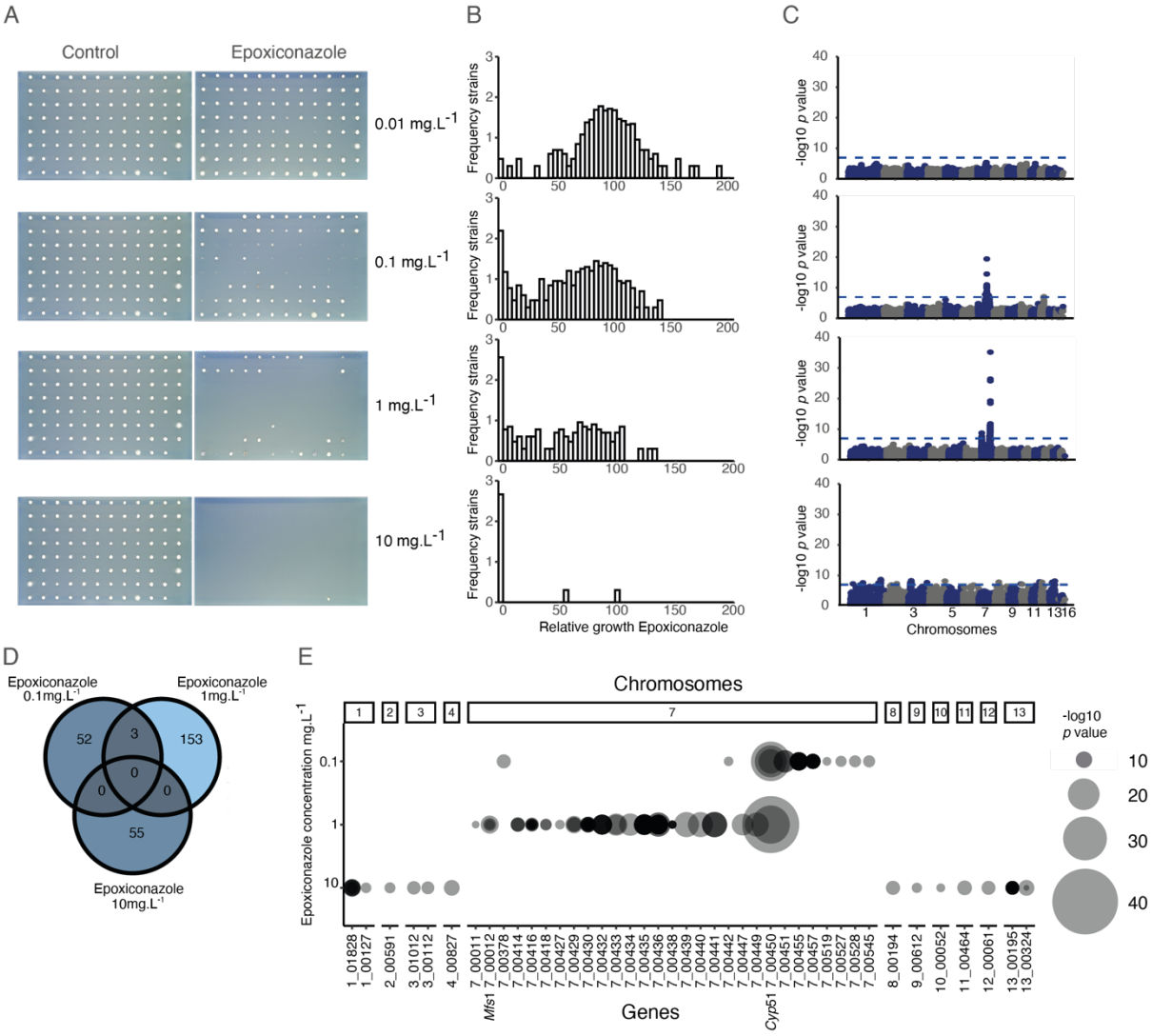

Figure 4: Relative colony growth resistance phenotyping and association mapping (A): Colony growth in presence of fungicides at 0.01, 0.1, 1, 10 mg.L^{-1}. (B): Frequency distribution of relative colony sizes. 0 corresponds to no growth and 100 corresponds to equal growth on control and fungicide medium. C: Manhattan plots showing ignificant associations above the Bonferroni threshold (blue dotted line). D: Venn diagram of SNPs above the Bonferroni threshold. (E) Scatter plot *p*-values above the Bonferroni threshold overlapping with a gene detected for resistance assessments in concentrations 0.1, 1, 10 mg.L^{-1} of epoxiconazole and based on relative growth.

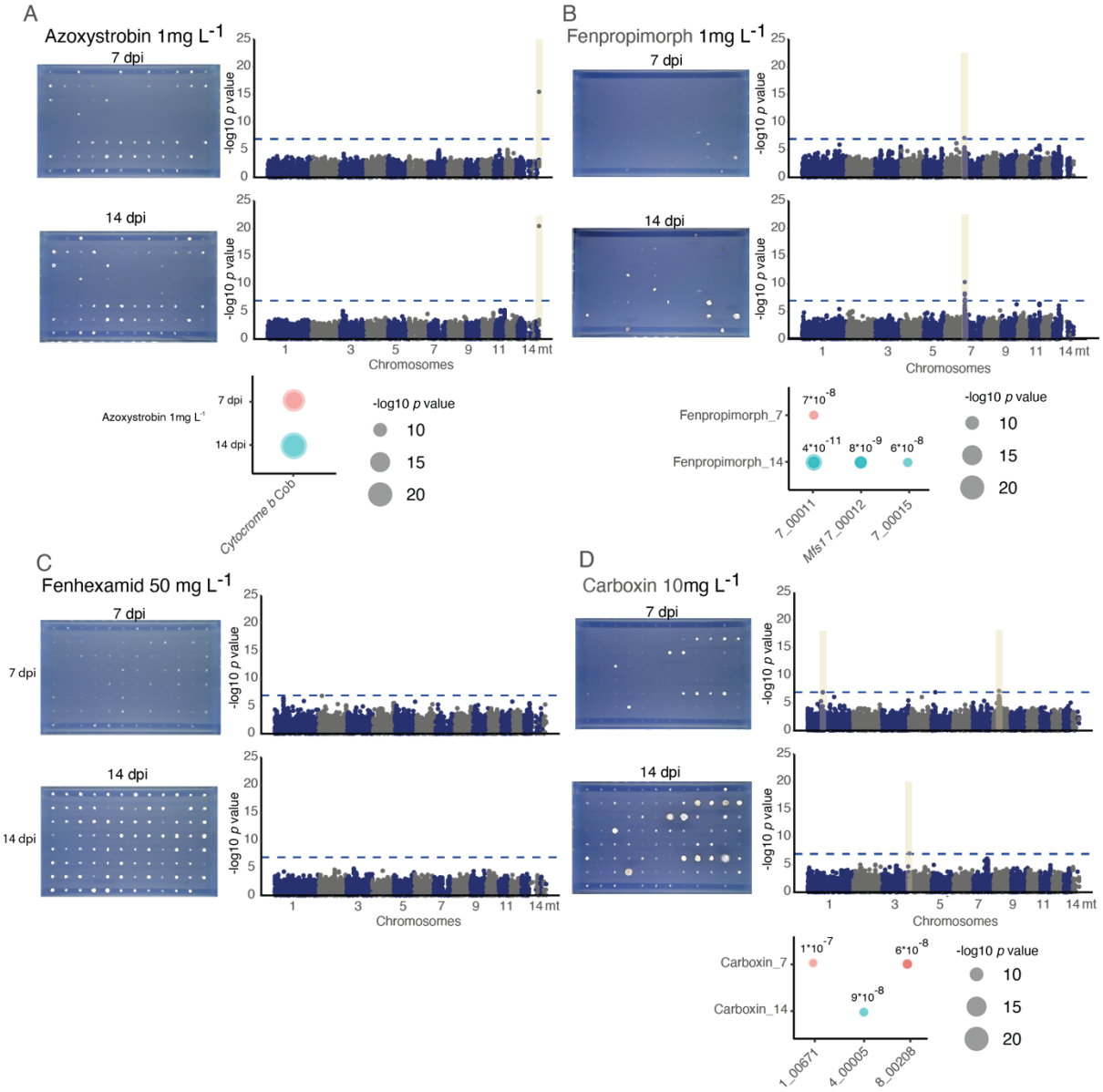

Figure 5: Relative colony growth resistance phenotyping and impact of colony age (7 vs 14 dpi). (A) Azoxystrobin (1 mg.L^{-1}), (B) fenpropimorph (1 mg.L^{-1}), (C) fenhexamid (50 mg.L^{-1}), (D) carboxin (10 mg.L^{-1}). The Manhattan plots show brown rectangles corresponding to regions with SNPs significantly associated with resistance. In the scatterplot, the blue color corresponds to SNPs overlapping with genes significantly associated for measurements at 7 dpi and red colors correspond to 14 dpi data.

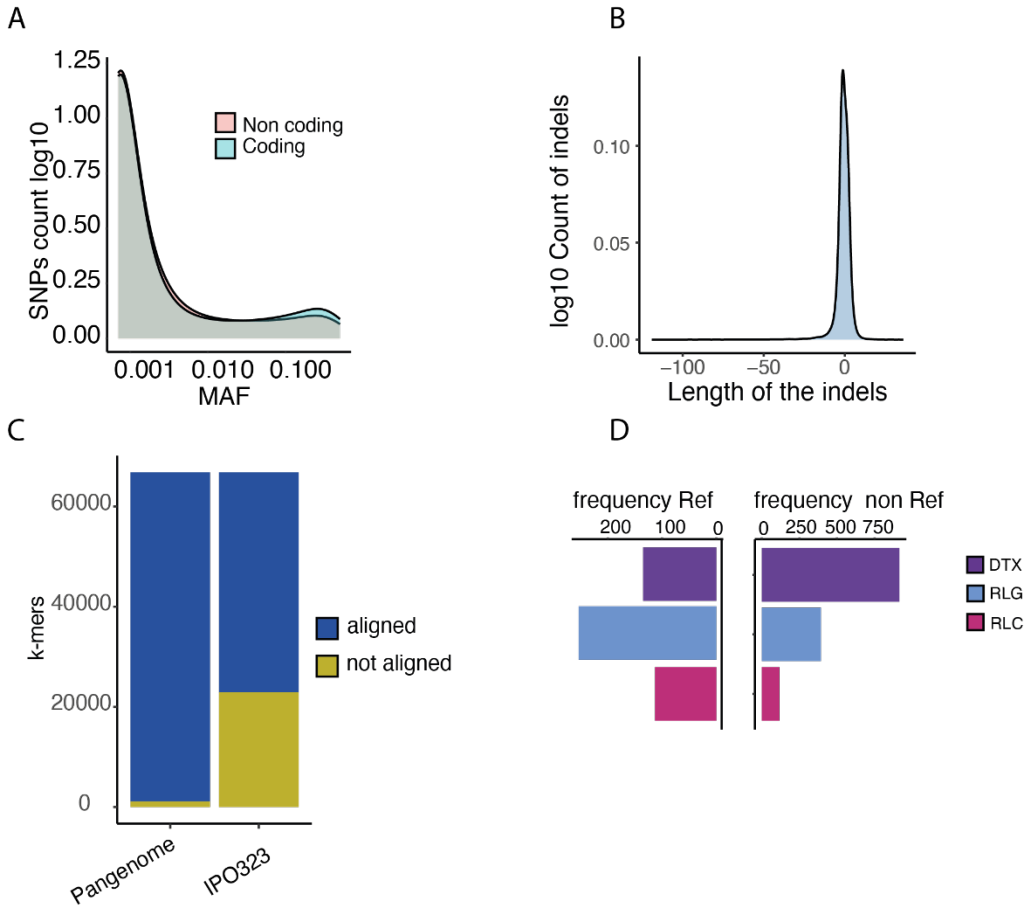

Figure 6: SNP and indel variant distribution in the European diversity panel. (A) Minor allele frequency distribution of coding and non-coding variants in the European diversity panel. (B) Indel length distribution. (C) Proportion of k-mers aligning (yellow) or lacking positioning (blue) on the reference genome (IPO323) and on the pangenome of the species. (D) Count of the most frequent TE superfamilies present in the European diversity panel split into reference and non-reference TEs.

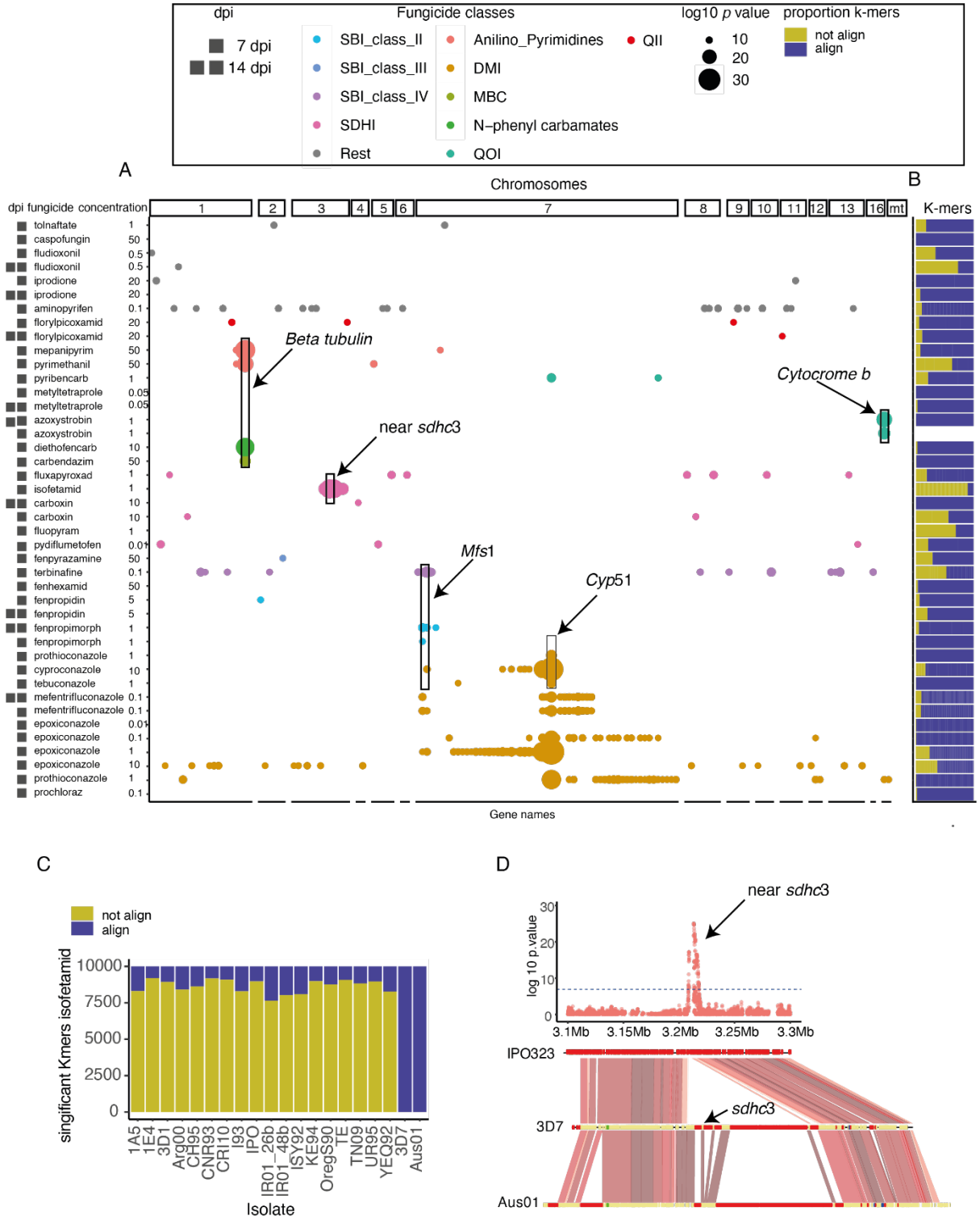

Figure 7: Construction of a SNP and k-mer based fungicide resistance atlas. (A) Scatter plot of SNP *p*-values above the Bonferroni threshold overlapping with genes and for the 43 assays based on relative growth. Fungicides are grouped and colored based on classes: SBI class II, SBI class III, SBI class IV, SDHI, anilino-pyrimidines, DMI, MBC, N-phenyl carbamates, QII, QOI, and others (corresponding to PP-fungicides, dicarboximides, carbamothioic acid derivative, echinocandin, 2-aminonicotinate). (B) Proportion of k-mers aligning (yellow) and not aligning (blue) on the IPO323 genome. (C) Proportion of aligned and un aligned significant k-mers for isofetamid on the species pangenome. In blue, aligning; in yellow, proportion not aligning to the pangenome. (D) Manhattan plot for the chromosome 3 of positions 3.1-3.3 Mb and a synteny plot of the same region represented by the

reference genomes Aus01 and 3D7 strains highlighting the rearrangement of the locus. In red, TEs; in yellow, annotated gene regions.

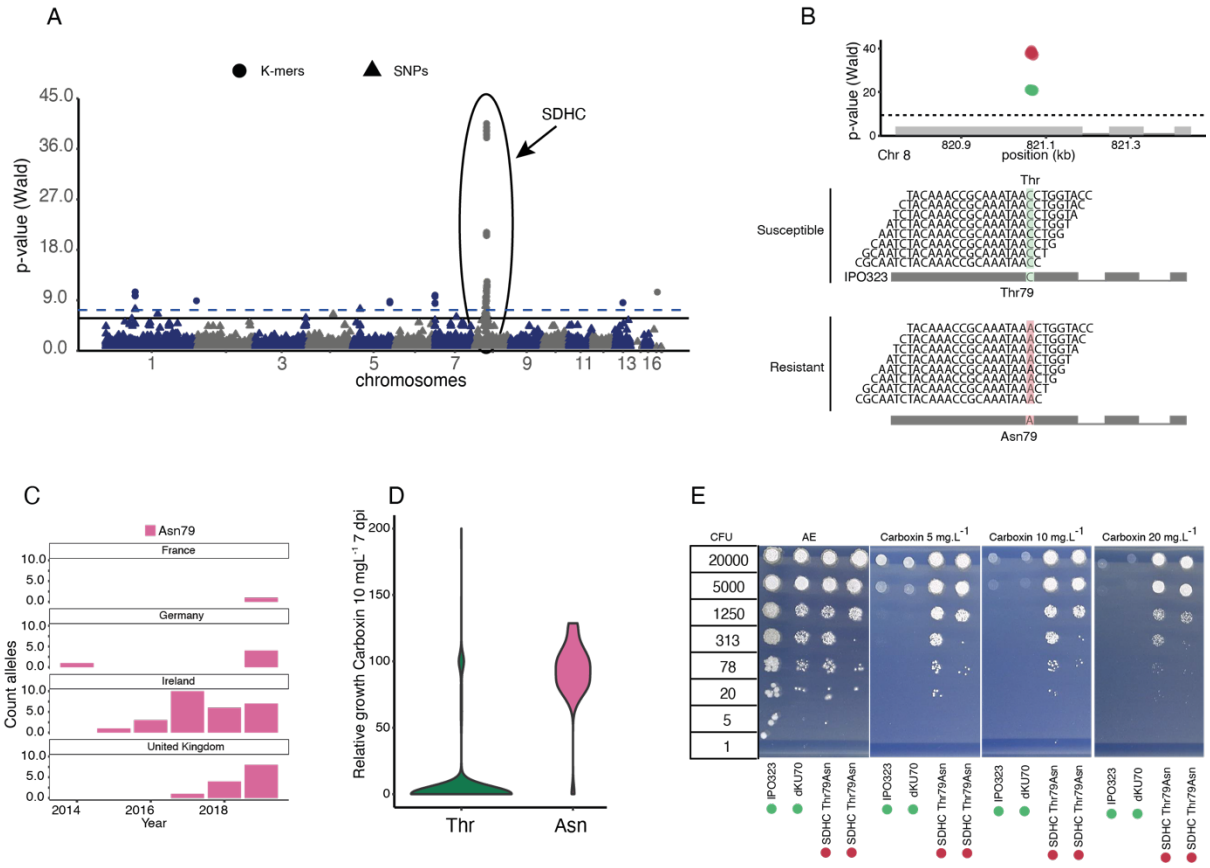

Figure 8: Profiling and functional validation the Thr79Asn variant in *SdhC1* associated with carboxin resistance. (A) Manhattan plot of carboxin resistance variants (10 mg.L^{-1}) with k-mers (circles) and SNPs (triangles). (B) Zoom on the k-mers mapping to the *SdhC*1 gene region at 820.7-821.4 kb on chromosome 8. Multiple sequence alignment of k-mers matching either the Thr residue (in green) or Asn (in red) at the codon position 79. (C) Frequency of the Asn residue across the European diversity panel. (D) Violin plot comparing relative growth values in strains with Thr and Asn. (E) Functional validation of mutants shown on a spotting assay including IPO323 (wild type), dKU70 (green dots) and SDHC_Thr79Asn (red dots) on AE media amended with carboxin at 5, 10, 20 mg.L^{-1}.

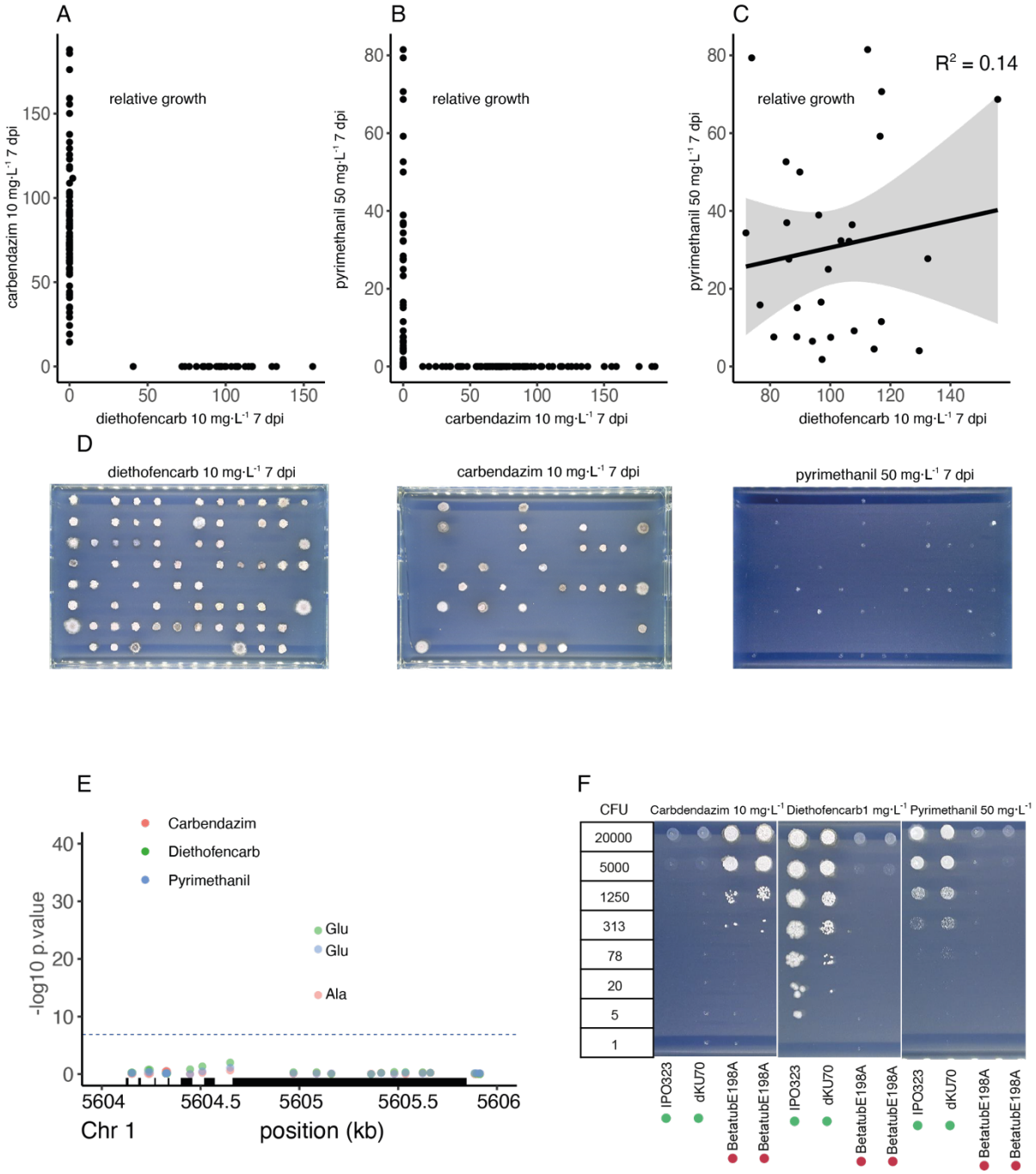

Figure 9: Profiling and functional validation of the Glu198Ala variant in *beta-tubulin* associated with pyrimethanil, diethofencarb, and carbendazim resistance. (A) Correlation of relative growth values between carbendazim and diethofencarb. (B) Correlation of relative growth values between pyrimethanil and carbendazim. (C) Correlation of relative growth values between pyrimethanil and diethofencarb. (D) Fungal colonies in the presence of pyrimethanil (50 mg.L^{-1}), diethofencarb (10 mg.L^{-1}), and carbendazim (10 mg.L^{-1}). (E) Zoomed Manhattan plot of significant SNPs for pyrimethanil, diethofencarb, and carbendazim, highlighting the *beta-tubulin* gene region (506.4–506.6 kb) on chromosome 1. Each significant SNP is labeled with the resistance-associated allele (Thr or Asn). (F) Functional validation of the mutants shown on the spotting assay with IPO323 (wild type), dKU70 (green dots), and SDHC_Thr79Asn (red dots) on AE medium amended with pyrimethanil (50 mg.L^{-1}), diethofencarb (1 mg.L^{-1}), and carbendazim (10 mg.L^{-1}).

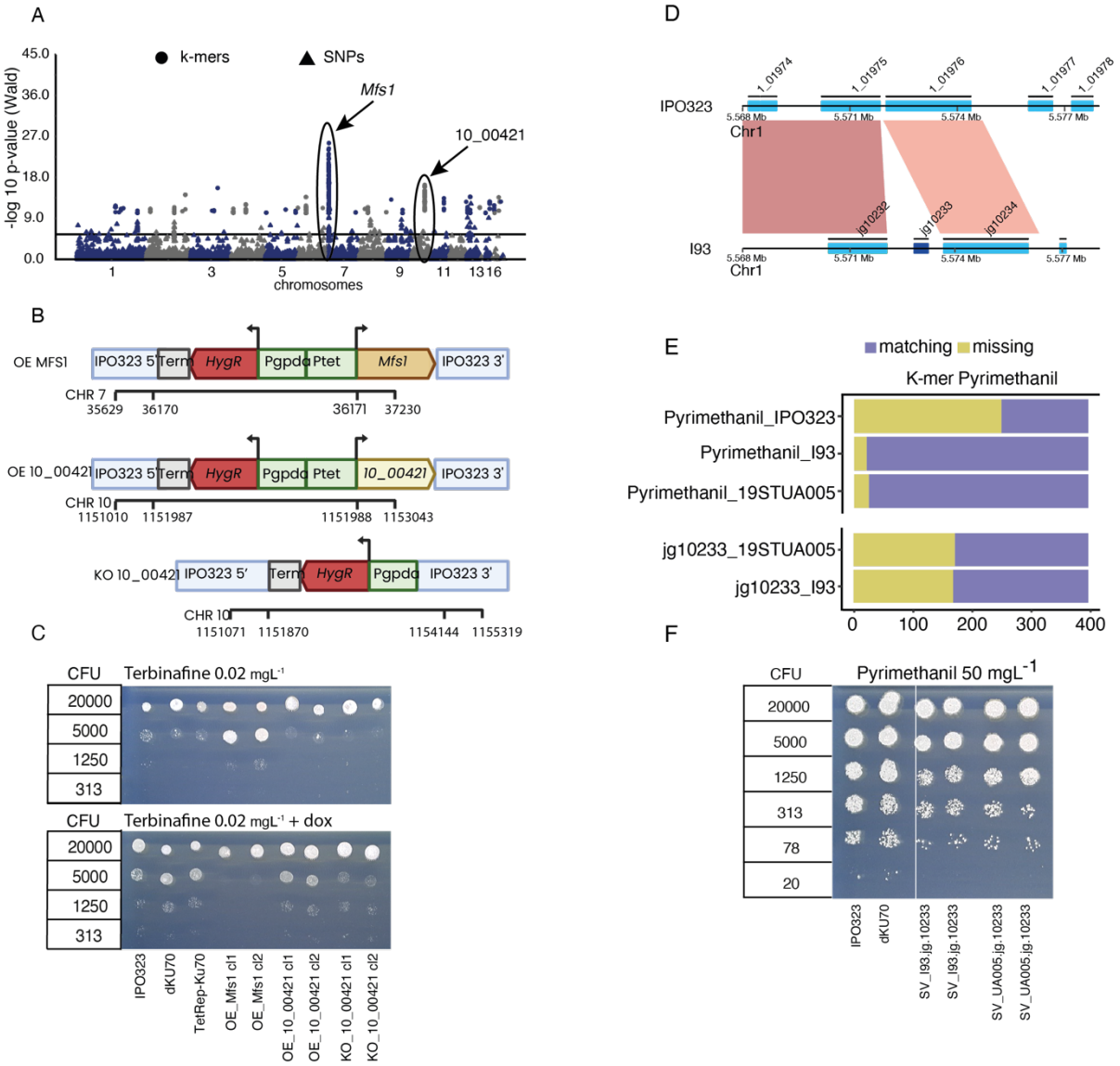

Figure 10: Profiling and functional validation of the role of the 10_00421 gene in terbinafine resistance. (A) Manhattan plot of significant SNPs (triangle) and k-mers (dots) for terbinafine relative growth values (0.1 mg.L^{-1}). Shapes identify variant types including SNPs (dots) and k-mers (triangle). (B) Construct design of OE_MFS1, OE_Zt09_10_00421, and KO_Zt09_10_00421 and (C) spotting assays on terbinafine (0.02 mg.L^{-1}), with and without doxorubicin (dox) (at 30 mg.L^{-1}). (D) Synteny plot of the chromosome 1 (5.568-5.577 Mb) of genomes IPO323 and I93. In light blue, gene regions; in dark blue is the gene jg.10233. (E) Proportion of k-mers aligning (yellow) or not (blue) to the genomes of IPO323, I93, and 19UA005; proportion k-mers aligning (yellow) or not (blue) to the structural variant (SV) affecting the gene jg.10233 in the strains I93 and 19UA005. (F) Spotting assay for pyrimethanil concentration (50 mg.L^{-1}).